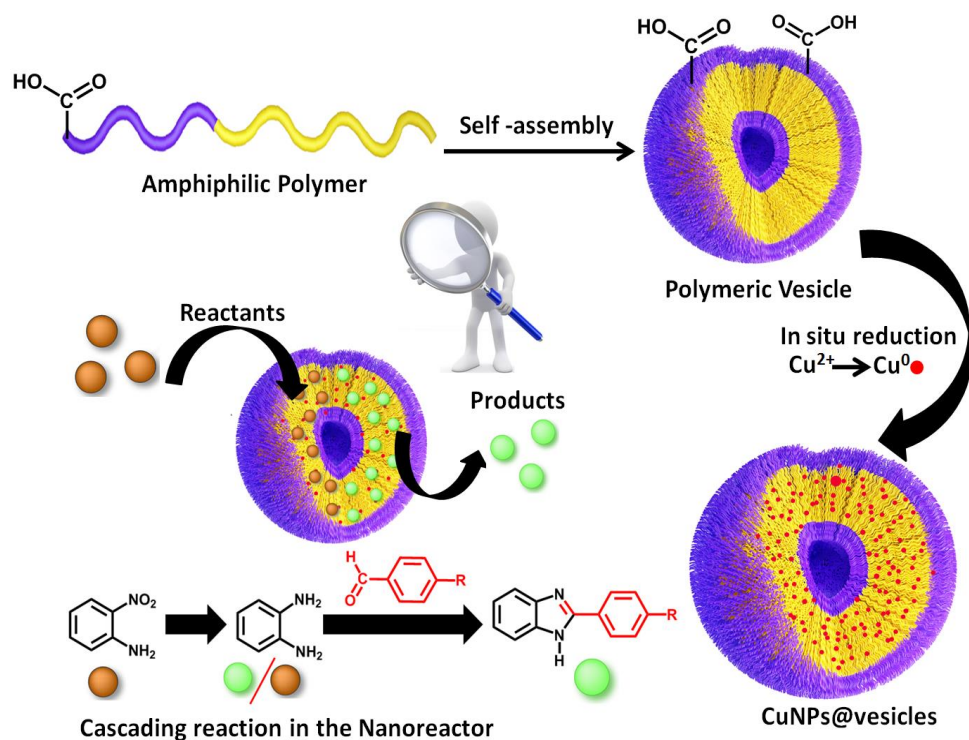# Chapter 4

Copper nanoparticles loaded polymer vesicles as environmentally amicable nanoreactors: A sustainable approach for cascading synthesis of benzimidazole

4.1 Introduction

Reactions in aquoues medium are desirable from environment perspective. The quest for newer nanocatalysts that perform in aquoues medium lead us towards micellar systems. Polymersomes are assemblies of amphiphilic copolymers in aqueous medium which bear resemblance to liposomes. These polymersomes exhibits unique morphology, with a hydrophobic membrane and a hydrophilic corona mediating a non-covalent self-assembly. Due to distinct hydrophilic and hydrophobic pockets, polymersomes are excellent auxiliaries for potential applications in drug delivery [1], [2], [3]and waste water remediation [4]. The success of employing polymersomes for aforementioned applications is due to their stability, robustness and potential of advanced chemical functionalization. This has motivated researchers to design polymersome derived nanoreactors for applications in catalysis.

Polymersomes with various morphologies like micelles [5], [6], vesicles [4], [7], [8], [9], micro emulsions [10], [11] etc. have been known to serve as nanoreactors for organic transformations. However, reports of literature suggest that vesicles are more efficient nanoreactors as compared to other nanoassemblies. This is because polymeric vesicles not only protect the catalyst within its compartments, but also facilitates a facile on-site isolation of reactive compounds enabling cascade reactions. They possess the ability to convert hydrophobic substrates in water and allow catalyst recovery. Such polymer vesicles can also encapsulate hydrophobic molecules and offer surfactant free metallovesicle assemblies [12].

With suitable functionalities polymer vesicles can also support metal nanoparticles encapsulation resulting in metallovesicles formation. Such metallovesicles can aid to adopt an approach where reactions can be performed under relatively mild conditions. For instance, Sun et. al., have demonstrated the potential of silver decorated homopolymeric vesicles to reduce water insoluble *p*-nitrophenol in aqueous media [13].In yet another report, Jianzhong Du and co-workers have reduced 4-nitrophenol (4-NP) using Au encapsulated vesicles [14].This is a crucial development, as nitroaromatics have been listed as "priority pollutants" by US EPA and its straightforward hydrogenation into its amino analogue can be a green strategy [15], [16], [17], [18],[19].

Metallovesicles capable of performing cascade reactions can further be deployed to convert these amino derivatives into organic compounds of commercial importance. Thus, fabrication of metallovesicle with appropriate rationale can turn out to bring a new advent in sustainable chemistry due to their ubiquitous assistance in synthesis of commercially important compounds.

With this background, our attempts were directed towards the synthesis of benzimidazole and its derivatives (N-containing heterocyclic compound) as they have significant applications in pharmaceuticals industries, dyes and chemo sensing UVB filters, florescent devices, etc. Previous research in the area suggest that precious and rare transition metals (Ru, Rh, Ir, Pd etc.)[20],[21]and copper derived hybrid materials are effective catalysts for synthesis of benzimidazoles. The performance of some homogeneous and heterogeneous catalysts such as $\{Mo_{72}V_{30}\}$ nanocluster [22], Co-ZIF-67 [23], SDS micelles [24], $CeCl_3.7H_2O$-CuI [25],bimetallic Cu-Mn B spinel oxide [26],$CuFe_2O_4$nanoparticle [27] recently reported has been summarized in **Table 4.6**. The classical approach of synthesis suffers from various limitations such as use of expensive catalysts, harsh reaction conditions (bases and toxic solvents) [28], formation of undesirable and hazardous by-products [29], [30]. Low yields, difficulties in product separation and lack of catalyst recyclability are also identified as key limitations [31]. The reaction also suffers from poor selectivity resulting in the formation of 1, 2-disubstituted benzimidazole along with 2-substituted benzimidazole as a mixture [24].

Recent reports suggest that polymersome mediated catalysis can help to overcome these limitations. Kaur et. al., for instance, have reported synthesis of benzimidazole derivatives with metallosurfactant catalyst, loaded with copper ions, under mild conditions [32]. This is a report on successful micellar catalysis. However, a cascading synthesis of benzimidazole has not been reported so far. Based on these findings, we propose the synthesis of a carboxyl functionalized polymer vesicles to develop metallopolymer nanoreactors loaded with copper nanoparticles (CuNPs).

Compartmentalization of copper ions within the polymeric vesicle leads to a fine balance between stability and surface activity. Metallovesicles offer enhanced reactivity and dual properties; the selectivity of a homogenous catalyst and recyclability of a heterogeneous catalyst [32]. Further, they are easy to synthesize effective at low loading, facilitate aqueous catalysis and pose minimal toxicity to the environment. Under the influence of "nano to nano effect"[33] a cascading reaction pathway can be achieved within the hydrophobic membrane of metallovesicles wherein reduction and the cross coupling reactions can occur. Metallovesicles also have the inherent benefits such as ease of separation/purification of the products along with recyclability of the catalyst.

In the past we have demonstrated the efficiency of hybrid nanocatalysts for reduction of nitroaromatics [34], [35]. Since nitroaniline is the precursor of benzimidazole, the ultimate aim

was to achieve cascading catalysis as well as selectivity as a result of structural complexity of metallovesicles that prevents side reactions and improves the reaction rate. Such a surfactant free Cu NPs encapsulated true polymeric vesicle as a catalyst system for a cascading and sustainable C-N coupling reaction has not been reported so far to the best of our knowledge.

4.2 Experimental Section

4.2.1 Materials

Dimethylolpropionic acid (DMPA), Hexamethylene Diisocyanate (HMDI), acetone, aldehydes and alcohols were purchased from Sigma Aldrich, India. Copper sulphate ($CuSO_4.5H_2O$), Ascorbic acid, o-phenylenediamine were procured from Sisco Research Laboratories (SRL), India. Sodium borohydride ($NaBH_4$), 2-nitroaniline (2-NA), and dimethyl sulfoxide were purchased from spectrochem India and calcein was purchased from Loba chemie, India. The dialysis bags (MWCO = 3000 Da) were purchased from Sigma Aldrich, India. Other reagents of analytical grade were purchased from commercial sources and used as received without further purification. The solutions were prepared using de-ionized water.

4.2.2 Characterization

Fourier Transform Infrared Spectroscopy (FTIR) spectra were recorded on a Bruker Alpha IR spectrophotometer at room temperature in the range of 4000-400 cm^{-1}. ^{1}H Nuclear Magnetic Resonance (NMR) and ^{13}CNMR spectra were recorded on Bruker Avance 400 MHz spectrometer using tetramethylsilane as an internal standard and $CDCl_3$ or DMSO as solvents. High Resolution Transmission Electron Microscopy (HR-TEM) and Energy dispersive X-ray spectroscopy (EDS) was recorded on Joel (Jem-2100F) electron microscope at 200 kV. For HR-TEM analysis, the CuNPs@vesicles solutions were diluted at ambient temperature and dispersed on a carbon coated copper grid. The grids were air dried under ambient temperature environment overnight. Imaging was recorded using Jeol (Jem-2100F) electron microscope at 200 kV. Dynamic light scattering (DLS) was used to determine the hydrodynamic diameter and polydispersity of vesicles in the solution which was performed on Beckman Coulter Delso Nano. Atomic Force Microscopy (AFM) and Field Emission Gun-Scanning Electron Microscopy (FEG-SEM) were recorded on NTEGRA PRIMA, NT-MDT, Russia and JSM-7600Frespectively. The florescence imaging of dye encapsulated vesicles was carried out. The fluorescence images were captured on a NikonTI2E live imaging fluorescent microscope. UV-vis spectrophotometric determinations were done using Perkin Elmer Lambda 35 and Fluorescence spectra were scanned on JASCO FP-

6300**.** The quantification of copper in the catalyst as well as in the supernatant was performed by atomic absorption spectroscopy (AAS) on an AA 6300: Shimadzu (Japan) atomic absorption spectrometer using an acetylene flame. The optimum parameters selected for measurements are: wavelength 324.7 nm; lamp current 2mA; slit width 0.2 nm; and fuel flow rate 0.2 L min^{-1}.

4.2.3 Synthesis and characterization of amphiphilic polymer DMPA-HMDI

The polymerization was carried out by adding HMDI (1.19 ml) to a solution of DMPA (1.0 g, 0.00745mol) in THF (2 ml). The reaction mixture was maintained at inert atmosphere under continuous flow of nitrogen. To this mixture, a solution of DABCO (33.2 mg, $2.96X10^{-4}$mol) dissolved in 1 ml THF was added. The reaction was allowed to proceed for 5 hours at 60°C. After this, another 1.0 ml of THF was added to obtain a viscous liquid and the polymer was precipitated using diethyl ether. A sticky polymer was isolated (for 1g DMPA, 1.5 mg of polymer was obtained).

4.2.4 Assessment of self-assembly of the amphiphilic polymer:

To check self-assembly, the polymer was directly dissolved in DMSO (0.1 wt% of the polymer) and then subjected to extensive dialysis for removal of excess of DMSO prior to physical studies.

4.2.4.1 FTIR studies to prove self-assembly into vesicles:

Polymer solutions were prepared in methanol and water and the spectra were recorded by placing drops of polymer solutions between two CaF$_2$ windows (path length = 0.2 mm). The spectra were scanned in the range of 4000−600 cm^{-1} with wavenumber precision of 0.005 cm^{-1}, 24 scans were recorded at 25 °C.

4.2.4.2 Dye encapsulation studies

The polymer solution (1 ml, 0.1 wt %) was encapsulated with calcein dye (30 μL, $1X10^{-3}$mol L^{-1}) in DMSO and diluted upto 3 mL using water. The resulting solution was subjected to extensive dialysis against water (MWCO = 3000 Da) for 24 hours to eliminate the possibility of presence of any un-encapsulated dye molecule. This solution was analyzed using UV-vis spectrophotometric analysis which shows peak at 484 nm corresponding to λ-max of calcein. Later, emission spectrum was recorded using this solution and compared with absorption matched emission spectra of free dye in water.

4.2.4.3 Urea addition and DLS experiments for disassembly: Proof of concept for urethane linkage mediated vesicle formation

For spectrofluorometric studies, 5 mg of solid urea was added to a calcein encapsulated polymer solution used for studies as per section 3.2. Urea was completely dissolved by stirring prior to spectral measurements. For DLS measurements 0.1 wt % of polymer solution was treated with 5 mg urea. The DLS spectra were recorded before and after the addition of urea.

4.2.5 Synthesis of CuNPs@vesicle catalyst

The CuNPs@vesicles was prepared by dispersing DMPA-HMDI (7mg) polymer in 10 mL DMSO in Erlenmeyer flask at room temperature. Further, 1mL of $CuSO_4.5H_2O$ (0.1mol L^{-1}) was added slowly while stirring. The pH of solution was adjusted to 9 by adding few drops ammonia solution. Later 1 mL of ascorbic acid (0.2 mol L^{-1}) solution was added so as to readjust the pH to 3 under continuous stirring. Temperature of the resulting solution was increased to 80°C and stirring was continued for 15 minutes. The formation of copper nanoparticles was marked by the development of a characteristic wine-red color in the solution. The nanoparticles thus prepared were extensively dialyzed against water for 24 hours to remove excess of DMSO, unencapsulated nanoparticles and unreacted reagents.

4.2.6 Experimental procedures for catalytic reaction

The detailed description of the protocol followed for carrying out desired reactions using CuNPs@vesicles as catalyst is as follows:

4.2.6.1 General procedure for catalytic formation of o-phenylenediamine

The desired precursor o-phenylenediamine (o-PDA) was obtained by the catalytic reduction of 2-nitroaniline(2-NA) with $NaBH_4$in the presence of CuNPs@vesicles. In a round bottom flask 1.9 mL of catalyst solution was added to 1 ml solution of 10 mM 2-NA under stirring. To this mixture, 2 ml of freshly prepared $NaBH_4$ (15.8mmol) was added as a source of hydrogen and the reaction was allowed to proceed at 30°C.The progress of reaction was monitored using UV–vis spectrophotometer. The completion of reaction was marked by complete disappearance of yellow color. From the black mixture, the product formed was isolated using ethyl acetate as the solvent followed by the regeneration of the red metallopolymer catalyst.

4.2.6.2 General procedure for one pot catalytic synthesis of 2-aryl-1 H-benzimidazoles

A mixture of o-phenylenediamine (1 mmol,1 equiv) and aromatic aldehydes (1 mmol,1 equiv) was added to a round bottom flask containing CuNPs@vesicles (5 ml,1440 ppm) and water (10 ml). The mixture was stirred at 30$^\text{o}$C and the progress of the reaction was monitored by thin layer chromatography (TLC) at regular time intervals. The product precipitated out as solid from the reaction mass was filtered under vacuum. It was purified by repeated washings of deionized water and recrystallized using ethanol.

4.2.6.3 Recycling of the catalyst

While recycling the catalyst, the reaction mixture was filtered. Upon filteration CuNPs@vesicles solution separated as a filtrate which was further treated with diethyl ether (3X 5 ml) to extract the traces of unreacted substrates, if any. The purified CuNPs@vesicles solution was collected and used for assessment of recycling efficiency for the next cascading cycle.

4.2.7 Experimental procedures for synthesis of benzimidazole using aromatic alcohol

2-nitroaniline (0.3 mmol) and p-nitrobenzyl alcohol (0.9 mmol) were taken in a two neck round bottom flask and 5ml of the catalyst was added to it. N$_2$ gas was purged into this mixture to create an inert atmosphere. The reaction mass was heated to 170 ℃ in a controlled temperature oil bath for 24 hours. The progress of the reaction was monitored using thin layer chromatography (TLC). The reaction mixture was cooled to room temperature after its completion and extracted in ethyl acetate (3 x 10 ml). The ethyl acetate layer was washed with brine (5 ml), dried over sodium sulphate and concentrated under vacuum. The obtained product was purified using column chromatography (10-20% ethyl acetate in hexane) to give the desired product.

4.3 Result and discussion

4.3.1 Synthesis and characterization of catalyst

An amphiphilic co-polymer with carboxyl functionalities was synthesized using dimethylol propionic acid and hexamethylene diisocyanate with urethane linkages according to **Scheme 4.1**. This amphiphilic polymer comprises of hydrophilic units of dimethyl propionic acid and hydrophobic hexamethylene units from HMDI. The amphiphilic co-polymer was precipitated

from the reaction mass in diethyl ether and purified thrice via precipitation technique.
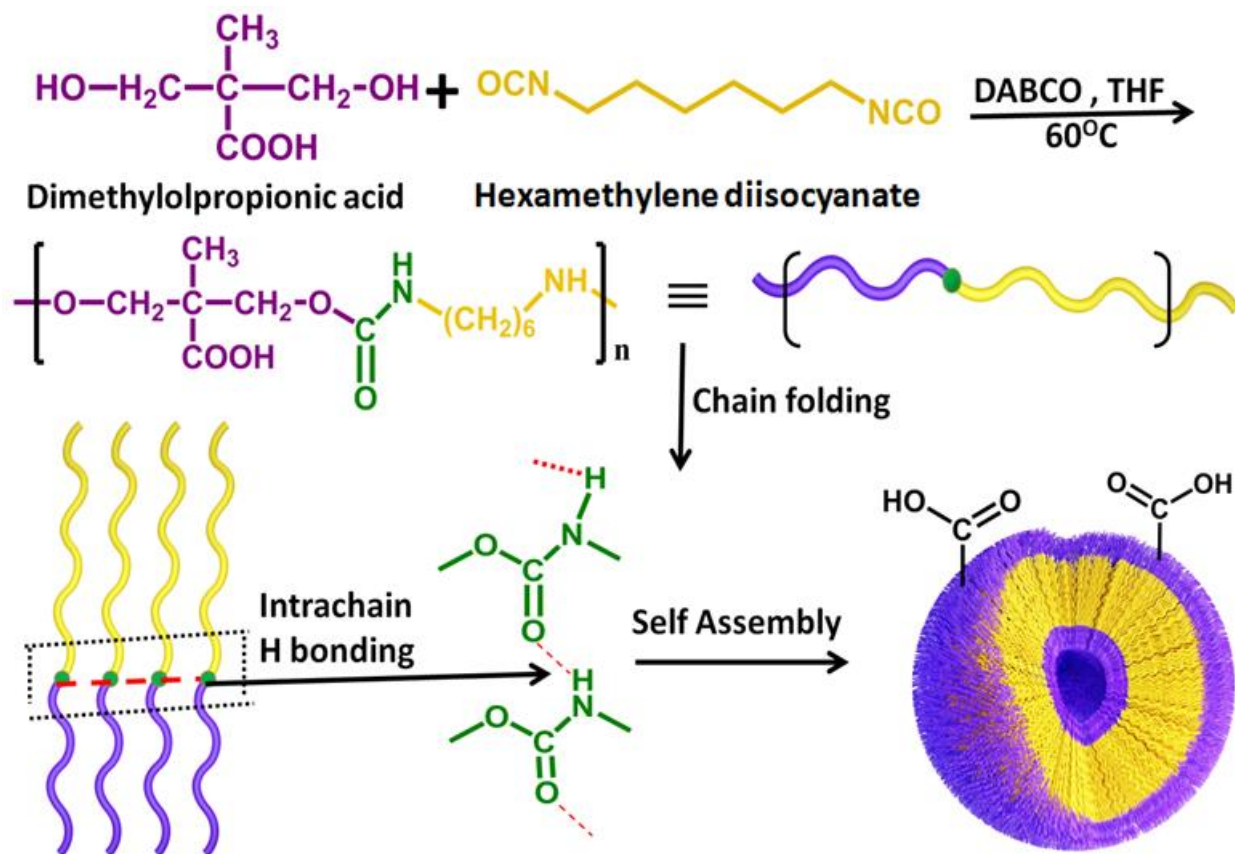
Scheme 4.1: Synthesis of amphiphilic DMPA-HMDI co-polymer and subsequent self-assembly into vesicle

The purified polymer was then analyzed with various spectroscopic techniques. For instance, the structure of the polymer was confirmed from ^{1}H NMR performed by dissolving the polymer in DMSO d^6. The δ value at 7.01 ppm corresponds to N-H proton of urethane linkage. A proton peak at 4.01 represents the C-CH$_2$, repetitive unit of dimethylolpropionic acid, 3.59 ppm due to (O-CH$_2$) protons and 2.91-2.93 ppm for (CH$_3$) protons. The -CH$_2$ protons corresponding to the repetitive unit of Hexamethylene diisocyanate were observed at 1.04-2.08 ppm. The proton of free carboxylic acid group appears at 12.54 ppm (**Figure 4.1**).
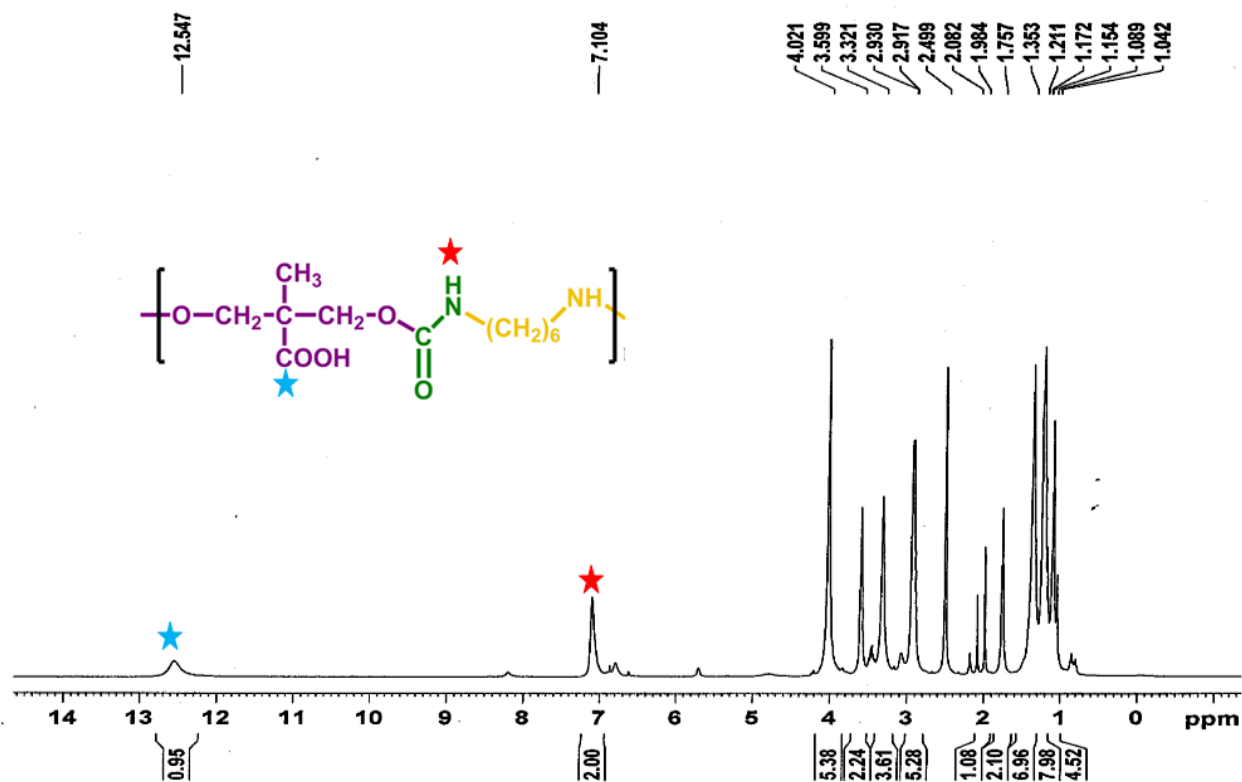
Figure 4.1: ^{1}H NMR of DMPA-HMDI polymer
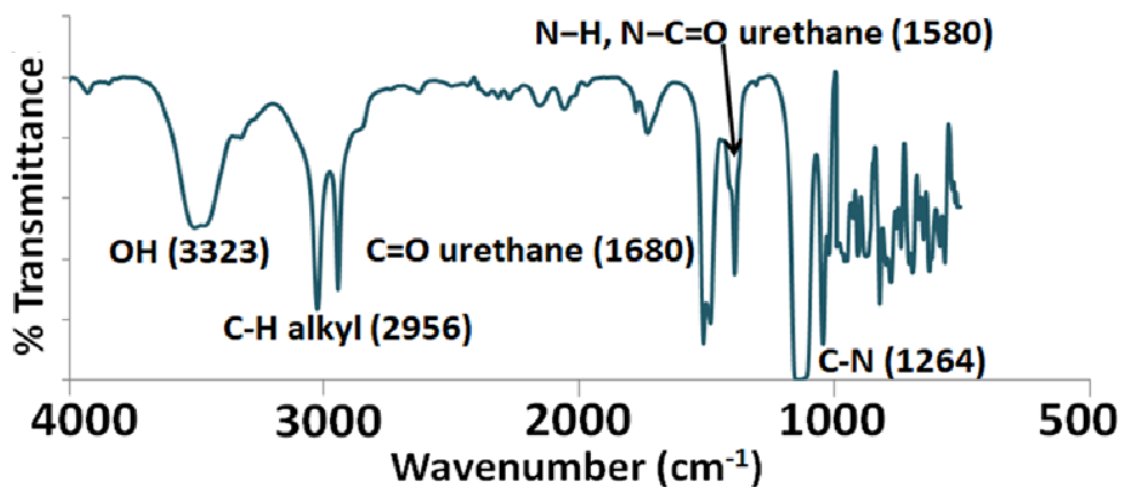
Figure 4.2: FTIR spectra (in KBr pellet) of DMPA-HMDI polymer

The data obtained from NMR spectroscopy corroborates with the FTIR spectroscopy. The characteristic peaks due to the presence of OH group and CH group were observed at 3323 cm^{-1}

and 2956 cm^{-1}respectively. The formation of urethane linkage was confirmed by the appearance of peaks at 1264 cm^{-1}, 1680 cm^{-1} and 1580 cm^{-1} representing C-N, C=O and N−H, N−C=O groups respectively **(Figure 4.2).**

An elemental analysis with EDAX determination suggests that the polymer contains 60wt% of C, 5wt% of N and 34 wt% of O (**Figure 4.3**).
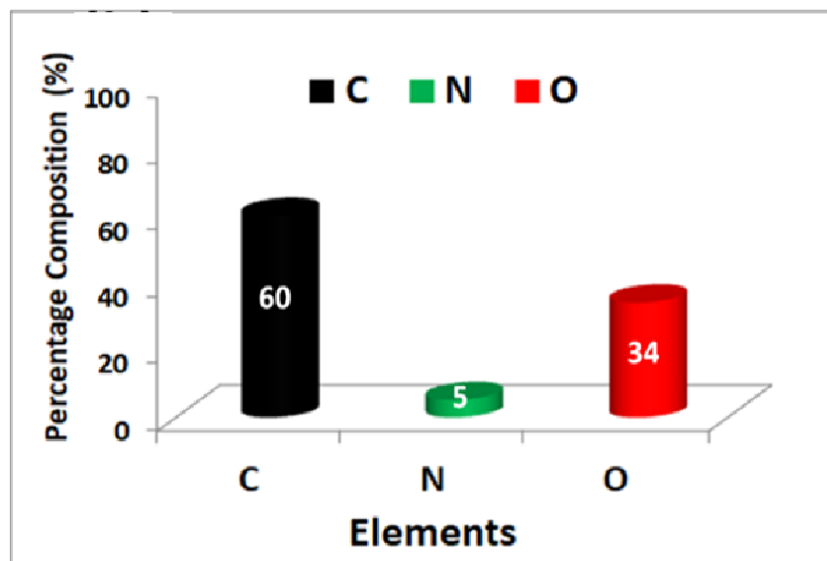
Figure 4.3: Elemental mapping of DMPA-HMDI polymer

After these structural characterizations, the ability of this amphiphilic co-polymer to self-assemble into vesicles was evaluated. It was observed that 0.7 mg/ml of polymer concentration was required for vesicle formation. To make this solution, 7.0 mg of the purified polymer was dissolved in 5 ml of DMSO. After this excess of DMSO was removed by extensive dialysis against water [13]. The self–assembly of amphiphilic copolymer is driven by the colloidal amphiphilicity [36]. To evaluate the formation of vesicles, via self-assembling, different studies were carried out i.e. FTIR, HR-TEM, AFM, FEG-SEM, DLS, fluorescent microscope imaging and fluorescence measurements. After these structural characterizations, the ability of this amphiphilic co-polymer to self-assemble into vesicles was evaluated. It was observed that 0.7 mg/ml of polymer concentration was required for vesicle formation. To make this solution, 7.0 mg of the purified polymer was dissolved in 5 ml of DMSO. After this excess of DMSO was removed by extensive dialysis against water [13]. The self–assembly of amphiphilic copolymer is driven by the colloidal amphiphilicity [36]. To evaluate the formation of vesicles, via self-assembling, different studies were carried out i.e., FTIR, HR-TEM, AFM, FEG-SEM, DLS, fluorescent imaging and fluorescence measurements.

The intrachain H-bonding formation assists self-assembly into vesicles. Vesicular assembly as proposed in **Scheme 4.1** is assumed to form a bilayer via folding of the hydrophobic polymer backbone. The folding is driven by intrachain H-bonding of the urethane linkages in the polymer network. To support this model, FTIR spectra of polymer was scanned in methanol and water (**Figure 4.4**).
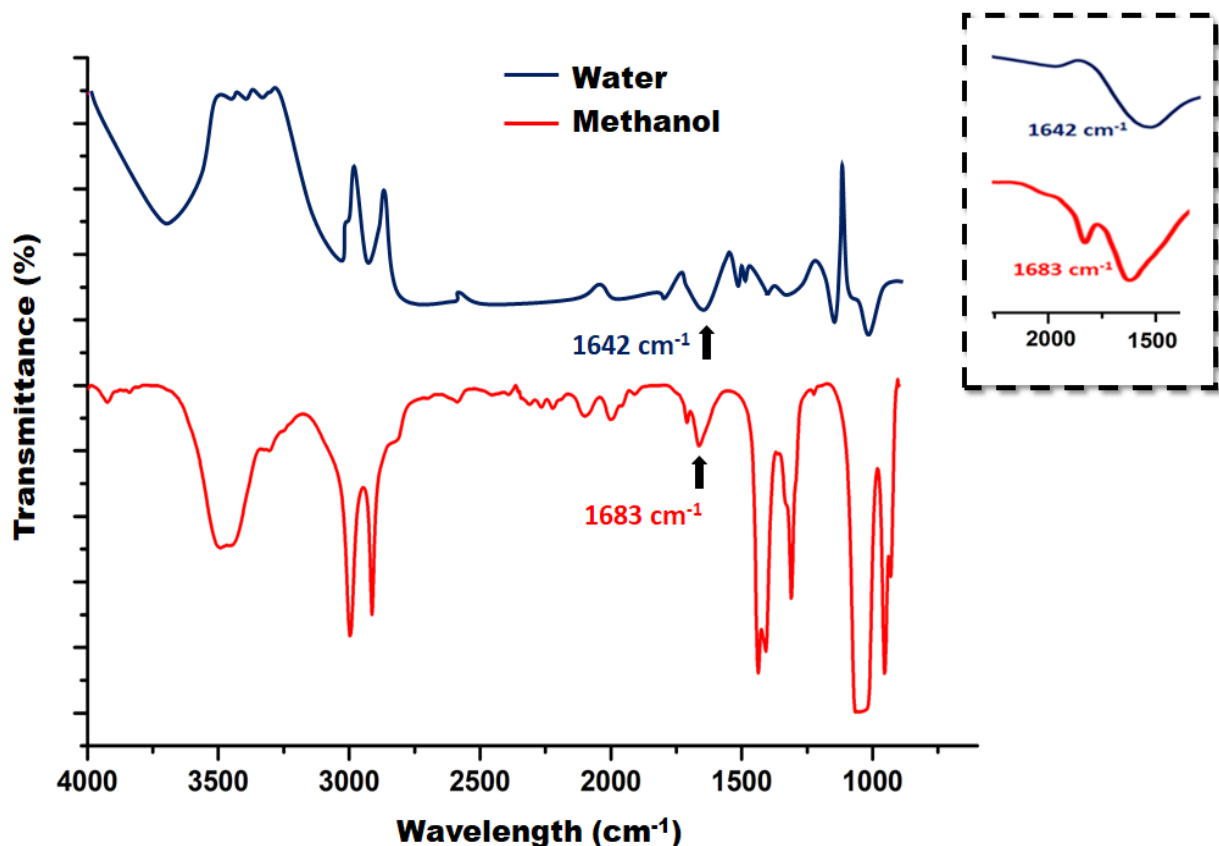
Figure 4.4: Various determinations by characterization techniques to prove self-assembly and disassembly (a) FTIR spectra in methanol and water

The peak corresponding to carbonyl stretching of urethane group which appeared at 1683 cm^{-1} in methanol was shifted by approximately 41 cm^{-1} in water and appears at 1642 cm^{-1}. This demonstrates the formation of H-bonding in water [37]. The vesicles exhibited a spherical morphology and presented diameters in range of 130-160 nm that has been confirmed via HR-TEM and FEG-SEM analysis. This is further confirmed from AFM determination wherein it was observed that the height of the assemblies(i.e, 20 nm) is less than its diameter (i.e, 140 nm), suggesting that they have spherical morphology [38] (**Figure 4.5**).
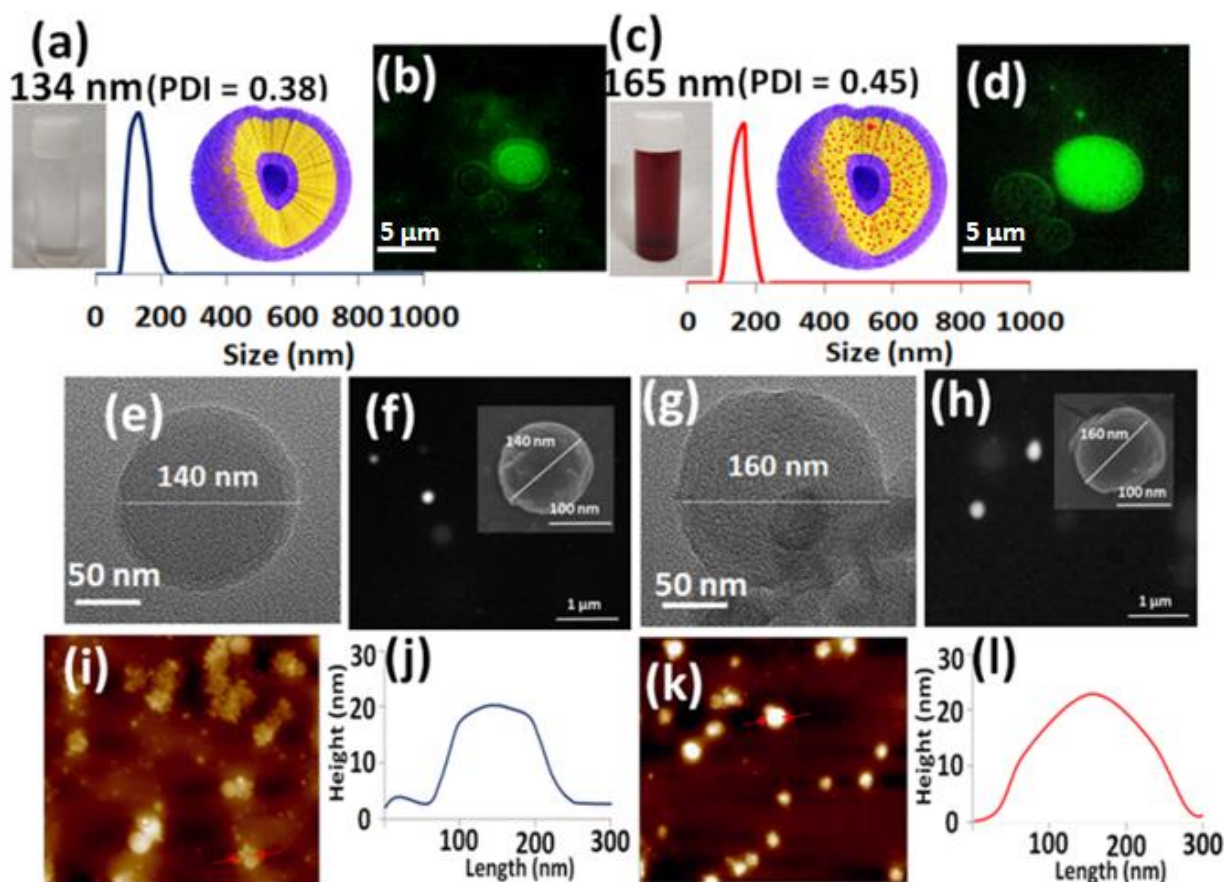
Figure 4.5: (a) Size distribution of the vesicles as observed in DLS histogram (b) florescent micrograph of vesicles (Inset: photograph of vial showing polymer solution)(c) DLS histogram depicting size distribution (d) florescent micrograph of CuNPs@vesicles (Inset: photograph of vial showing catalyst solution) (e) HR-TEM (f) FEG-SEM images of vesicles (g) HR-TEM (h) FEG-SEM images of CuNPs@vesicles (i),(j),(k) & (l) AFM images for vesicles and CuNPs@vesicles respectively. [Concentration of the samples was maintained as 0.1 mg/mL for all the measurements]

Vesicular morphology was confirmed by presence of water pool inside the self-assembled polymer [39]. This hypothesis was tested by the fact that hydrophilic dye molecules can be encapsulated within the hydrophilic interior. The extensively dialyzed solution demonstrated characteristics emission peak of calcein with $\lambda_{max} = 510$ nm (**Figure 4.5(b)**), indicating dye encapsulation. This emission intensity was compared to the absorption matched intensity of the free dye solution. The reduction in emission observed for calcein encapsulated in the confined water pool within the vesicle, is attributed to the phenomenon of self-quenching. The dye encapsulated solution examined under fluorescence microscope demonstrated bilayered green emitting spherical
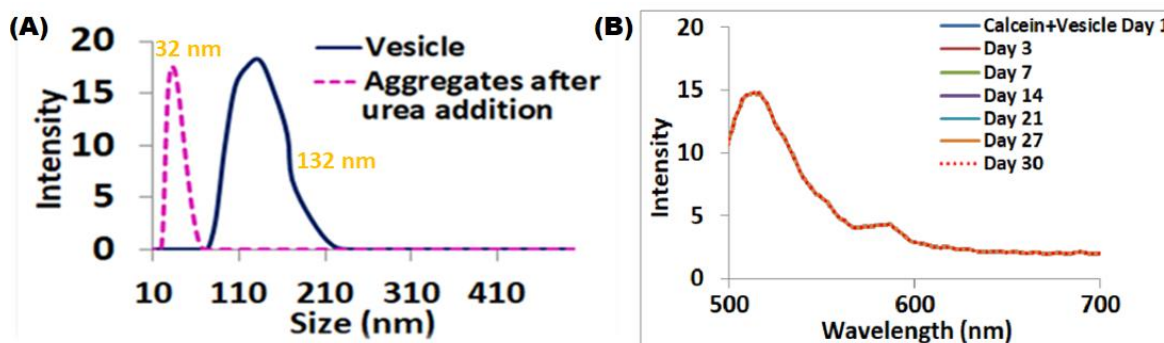
particles.
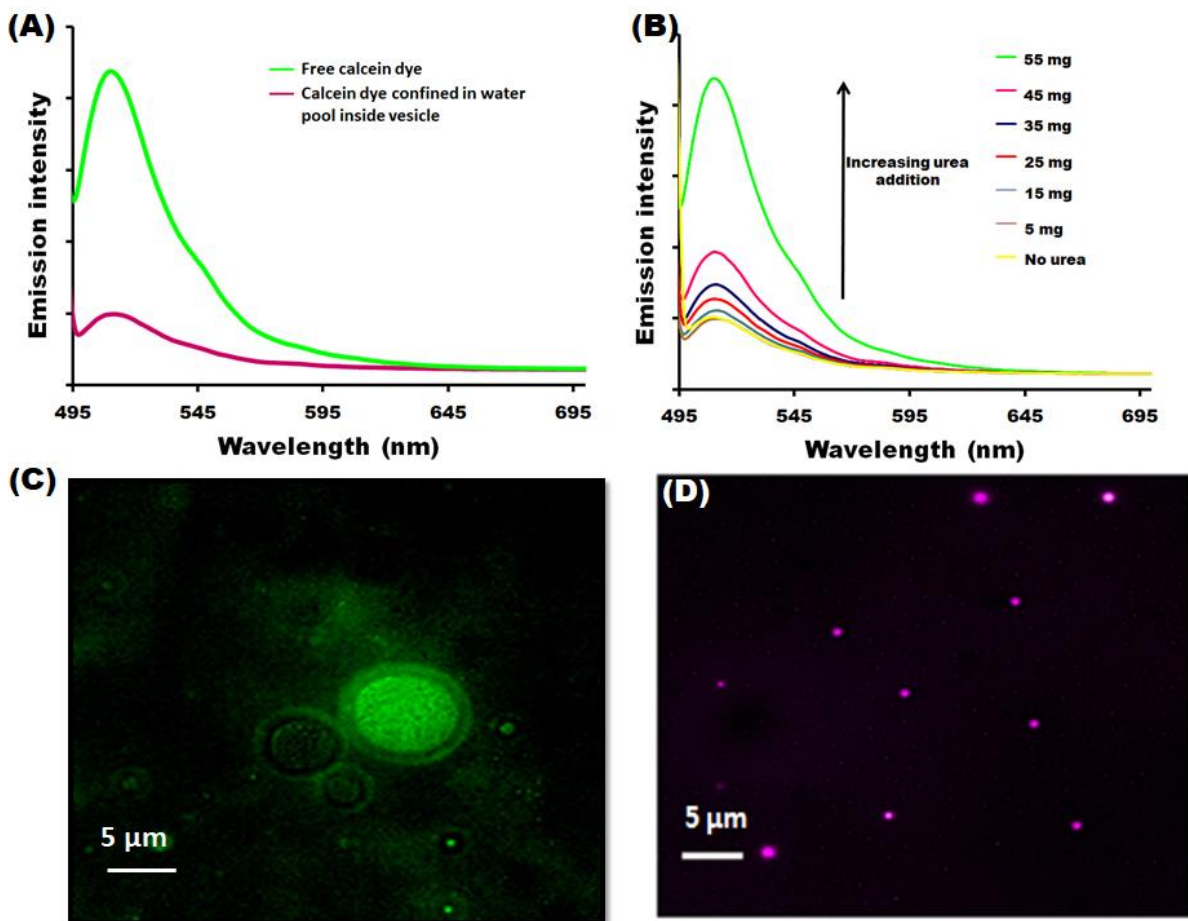
Figure 4.6: Various determinations by characterization techniques to prove self-assembly and disassembly (a) difference in the fluorescence intensities of calcein encapsulated vesicle and free calcein in water (b) Urea addition experiment (c) Calcein encapsulated vesicles and (d) Rhodamine b encapsulated vesicles in florescence study.

H-bonding-mediated self-assembled polymer undergoes denaturation in the presence of urea because it disturbs the H-bonding and thus the vesicles disassembled [40]. The self-quenching is due to confinement of dye molecules in the vesicle, addition of urea breaks the vesicle causing the release of dye molecules in bulk water and thus an enhancement in emission intensity (**Figure 4.6(c)**). This theory was further confirmed by DLS analysis. As shown in **Figure 4.6(d)** the polymer solution in absence of urea shows peak at 132 nm corresponding to presence of vesicles. This peak completely disappears upon urea treatment suggesting urea disassembly. On the contrary

a new peak is observed at 32 nm which may be due to formation of some undefined polymer aggregates **Figure 4.7(a)).** Further, calcein encapsulated vesicles captured via a fluorescence microscope exhibits a bilayered structure and the self-quenching studies further support their true vesicular nature [37]. The vesicles exhibit excellent kinetic stability upto 30 days as observed from fluorescence emission intensity of calcein **(Figure 4.7(b)).**

Figure 4.7: (a) DLS measurements showing disassembly of vesicles and (b) Calcein encapsulated vesicles showing stability upto 30 days as observed in florescence study.

Theoretical simulation studies performed via particle dissipative particle dynamics suggests that there exists a relationship between concentration of nanoparticles and the morphology of the self-assembling aggregate [41]. Upon an increased nanoparticle concentration, the co-polymers coalesce to form vesicles. With this purview, for the formation of metal encapsulated vesicles (i.e, Metallovesicles), the strategy of nanoparticle and copolymers co-assembly was adopted. For this the carboxylic acids existing as pendant groups in this amphiphilic co-polymer was employed for metal encapsulation. Thus, the carboxylic group not only renders adequate hydrophilicity for self-assembly but also aids in metal binding, exhibiting good catalytic activity and recyclability. The carboxyl functionalities on the bilayer of the vesicles ensures stronger interactions with the metal precursors to obtain highly dispersed copper nanoparticles [42,43].With this rational the copper sulphate ($CuSO_4.5 H_2O$) was used as the source of copper and ascorbic acid as reducing agent for subsequent reduction into nanoparticles **(Scheme 4.2)**.
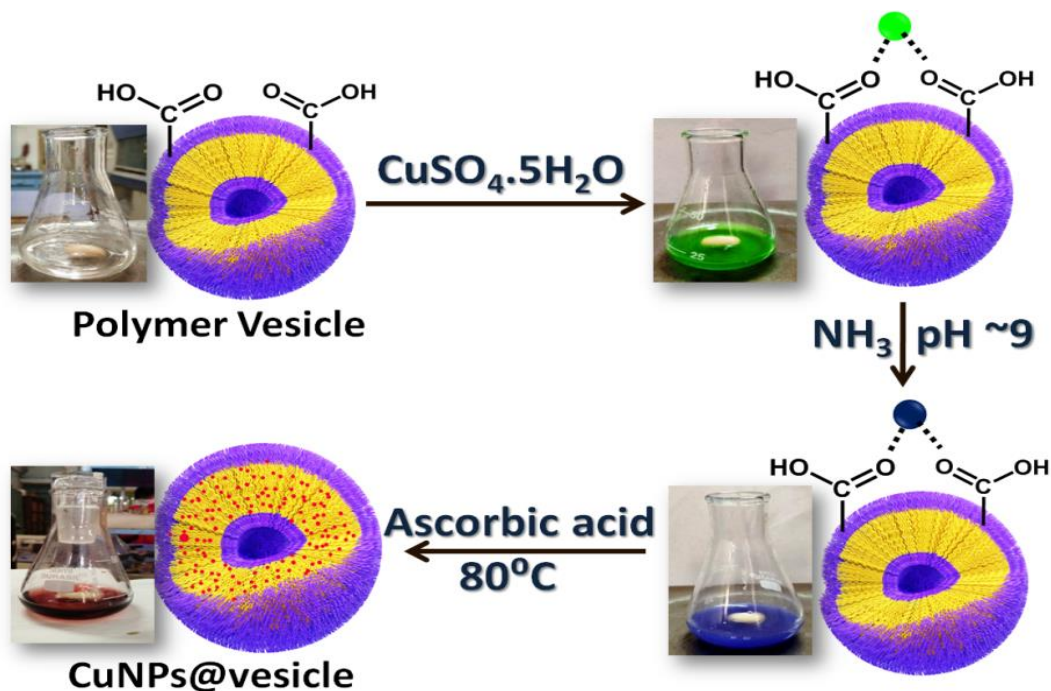
Scheme 4.2: Visual changes observed in the process of CuNPs@vesicles formation(i) bare vesicles (ii) binding of Cu^{2+} ions with vesicles (iii) Color change upon pH adjustment of the metal encapsulated vesicles and (iv) reduction and formation of Cu Nanoparticles.

Elemental mapping (**Figure 4.8**) confirms the presence and distribution of Cu in the vesicles while AAS analysis confirmed an encapsulation with 1440 ppm loading. The HR-TEM, FEG-SEM and AFM showed the size of the copper nanoparticles loaded polymeric vesicles is 160 nm, height was found to be 22 nm and morphology was observed to be spherical shown in figure 2. The formation of metallopolymer occurs as follows: The carboxylic functionalities on the vesicular bilayer assists Cu^{2+} adsorption [42]. This phenomenon was observed in the FTIR analysis, wherein the spectrum of the Cu ion containing vesicle solution shows peak at 447 cm^{-1}, a characteristic of M-O bond [44] .The Cu^{2+}ions trapped in the vesicles were then reduced to Cu nanoparticles using ascorbic acid. This led to disappearance of the M-O bond in FTIR spectrum of metallopolymer (as shown in **Figure 4.8**). The appearance of SPR band in the range 500 nm to 550 nm confirms formation of CuNPs.
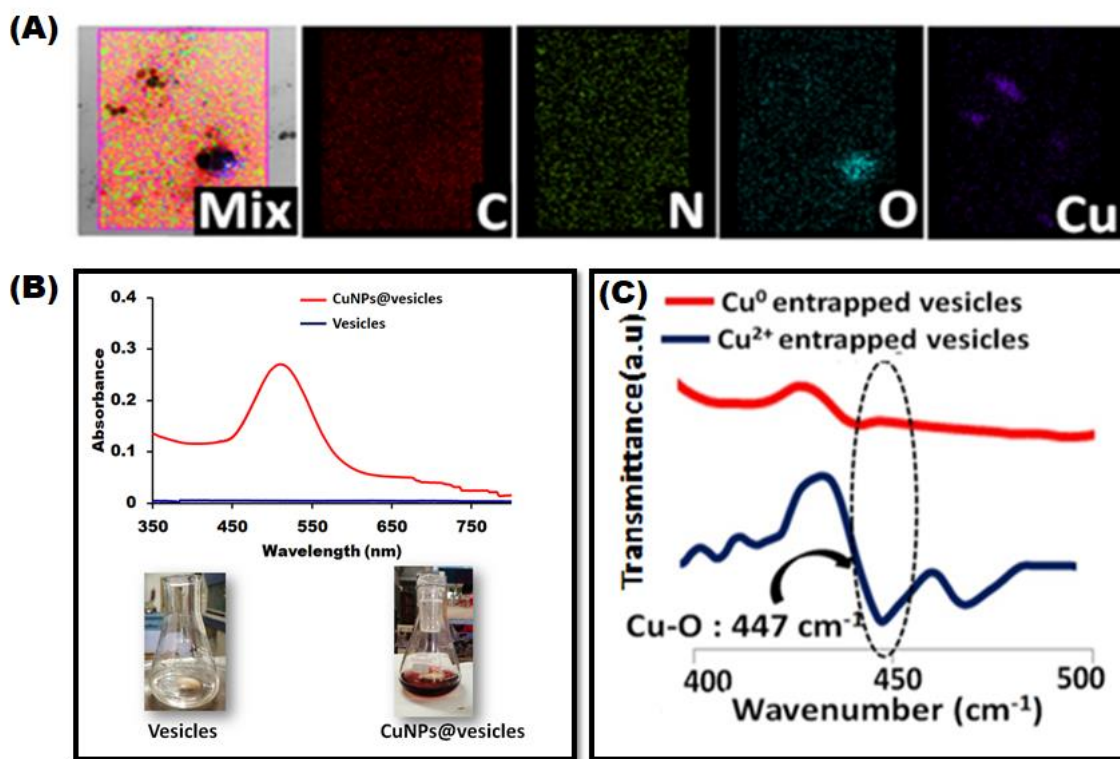
Figure 4.8: (A) Elemental distribution of CuNPs@vesicles as observed in EDAX mapping; C (red), N (green), O (blue) and Cu (purple) (B) A comparison of UV-vis absorption spectra for bare vesicles and CuNPs loaded vesicles (Inset digital images showing color transition due to Cu loading and (C) FTIR spectra showing binding of Cu^{2+} ions (blue line) in the vesicles and its reduction into nanoparticles (red line).

4.3.2 Role of CuNPs@vesicles as catalyst

4.3.2.1 Catalytic reduction of Nitroaromatics

The metallovesicles thus formed served as a nanoreactor which can encapsulate small hydrophobic molecules and whose interior houses CuNPs wherein an organic transformation can occur. The nanoreactor was employed for the synthesis of 2-substituted benzimidazole in a one pot environmentally benign synthesis via cascading pathway using easily accessible precursors (**Scheme 4.3**).
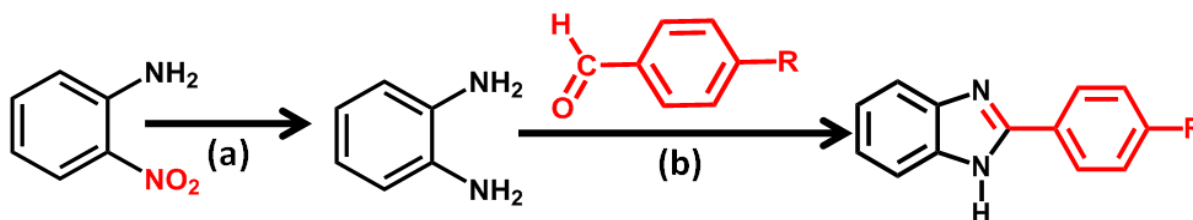
Scheme 4.3: CuNPs@vesicles catalyzed reactions for synthesis of benzimidazoles via cascading pathway. [Reaction conditions (a) catalyst 5 ml, NaBH$_4$, H$_2$O, 30 ºC (b) catalyst 5 ml, H$_2$O, 30 ºC]

The investigations began with initial optimizations to assess the activity of our catalyst towards the reduction of nitroaromatics using 4-Nitrophenol as model substrate to demonstrate the catalytic capability of CuNPs@vesicles. The UV-vis spectrophotometric monitoring demonstrated the successful reduction proceeding via 4-nitrophenolate ion intermediate formation **(Figure 4(a)).**

Table 4. shows the optimization experimental details such as effect of catalyst volume and sodium borohydride concentration for reduction of 4-nitrophenol. Control reactions were also carried out in presence of only NaBH$_4$. It was observed that even after 72 h reaction does not take place in the absence of catalyst.

Table 4.1: Effect of catalyst volume and water

Sr. No.	Volume of catalyst(ml)	Water (ml)	Time
1.	0.5	4.5	2 mins
2.	1.0	4.0	2 mins
3.	1.5	3.5	1 min
4.	2.0	3.0	30 sec
5.	1.6	2.4	60 sec
6.	1.8	2.2	40 sec
7.	**1.9**	**2.1**	**30 sec**

Table 4.2: Effect of concentration of sodium borohydride

Sr. No.	4-NP (mM)	NaBH$_4$ (mM)	Time
1.	0.1	5	10 mins
2.	0.1	10	6 mins
3.	0.1	15	2 mins
4.	0.1	20	38 seconds
5.	0.1	15.6	42 seconds
6.	0.1	15.8	40 seconds

To understand the role of nanovesicles in catalyzing the organic transformations, reaction was carried out in the presence of bare vesicles, bare CuNPs as well as in the presence of only CuSO$_4$.5H$_2$O (the precursor for CuNPs). In all these cases the product formation was observed after 20 h. It was observed that the isolation of product was difficult and the metal salt was not recyclable. This led us to conclude that the Cu nanoparticle loaded in the polymeric vesicles is the active component that drives the reaction which occurs within 30 seconds.

Table 4.3: Control experiment for reduction of 4-NP

Sr.no.	Catalyst	Amount of Catalyst (ml)	NaBH$_4$ (mmol)	Time
1	Bare vesicles	1.9	15.8	No reaction
2	CuSO$_4$.H$_2$O	1.9	15.8	20 h
3	CuNPs	1.9	15.8	24 h
4	CuNPs@vesicles	1.9	15.8	30 s

Reaction conditions: All the reactions were carried out at room temperature (30 °C), 4-Nitrophenol (10 mmol) and water (2 ml).

The reduction of 4-NP was also monitored, further, in the absence of NaBH₄ by taking only 4-NP and CuNPs@vesicles. Control reactions as shown in **Table 4.4** establish the fact that reduction doesn't proceed in the absence of catalyst. The reaction conditions optimized herein were further used for the reduction of 2-nitroaniline to yield o-phenylenediamine (o-PDA), which is the precursor for benzimidazole (**Table 4.4, entry 3**). To confirm that the encapsulated metal nanoparticles do not leach out as the reaction progresses, AAS studies of the reaction mass was carried out and no leaching was observed.

Table 4.4: Reduction of Nitroaromatics

Sr.no.	Reactant	$NaBH_4$ (mmol)	Catalyst (ml)	Time (seconds)
1	2-Nitroaniline	–	1.9	No reaction
2	2-Nitroaniline	15.8	-	No reaction
3	2-Nitroaniline	15.8	1.9	40
4	4-Nitrophenol	15.8	1.9	30
5	2-Nitrophenol	15.8	1.9	23

All the reactions were carried out at room temperature (30⁰C), Nitroarene substrates (0.1 mM), water (2 ml), catalyst 1.9 ml (CuNPs@vesicles) and sodium borohydride (15.8 mmol)
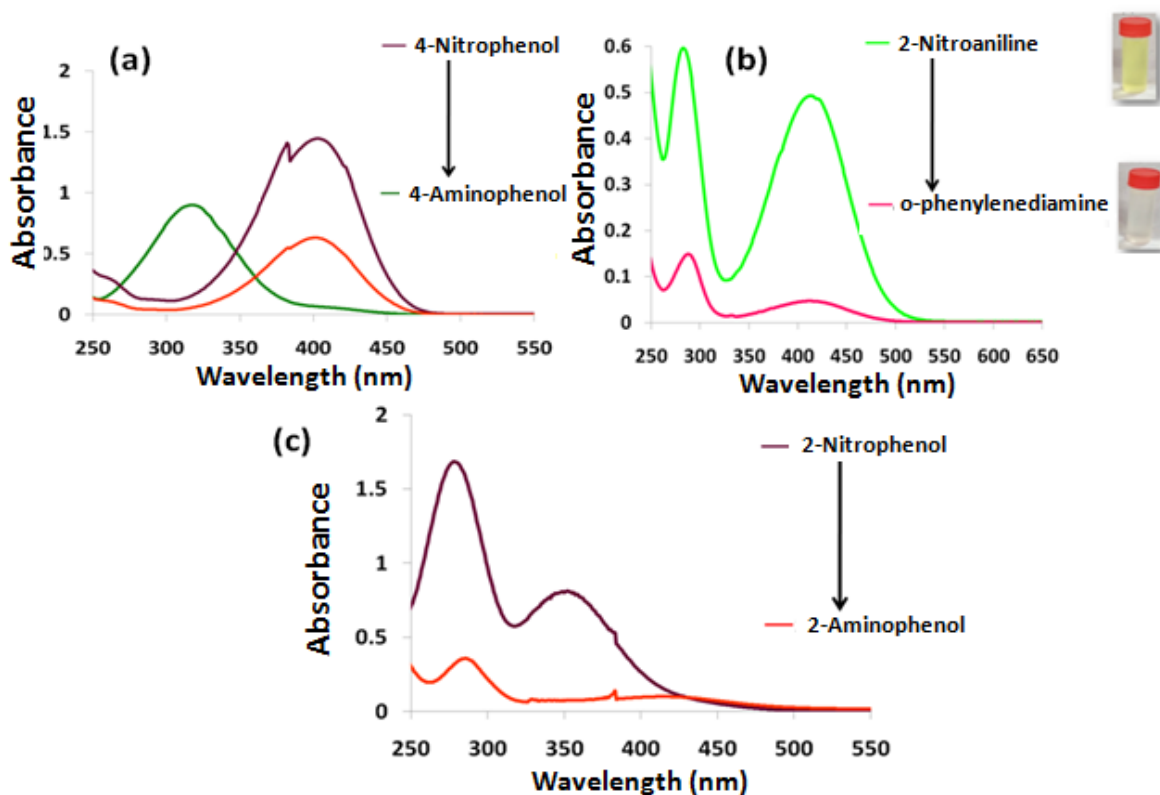
Figure 4.9: UV–visible absorption spectra of reduction of (a) 4-Nitrophenol (b) 2-Nitroaniline (c) 2-Nitrophenol

4.3.3 Catalytic synthesis of 2-substituted benzimidazoles

The CuNPs@vesicles was used to catalyze C-N coupling reactions using o-phenylenediamine and 4-nitrobenzaldehyde as model substrates, further. We observed that 90% isolated yield of the product {2-(4-Nitrophenyl)-1H-benzo[d]imidazole} was obtained within 30 minutes at ambient temperature (**Table 2, entry 1**). In the literature CuNPs have been used for the formation of benzimidazole, but they involve longer reaction time, formation of side products and use of toxic solvents[45]. However, employing CuNPs@vesicles for this transformation has enabled to carry out the reaction in water with significantly lower reaction time for complete formation of 2-substituted product. This is attributed to the vesicular nature of the present catalytic system wherein the amphiphilic polymer and Cu nanoparticles loaded therein functions synergistically to assist the conversion. The reactants are housed in the vesicular bilayer which helps to enhance its proximity with Cu NPs and necessary steric hindrance to avoid the formation of side products[32].

The optimization for C-N coupling reaction was further carried out by varying several parameters

like temperature and catalyst volume. It was observed that an increase in the volume of CuNPs@vesicles solution decreases the reaction time with increased product yield (shown in **Figure 5**).
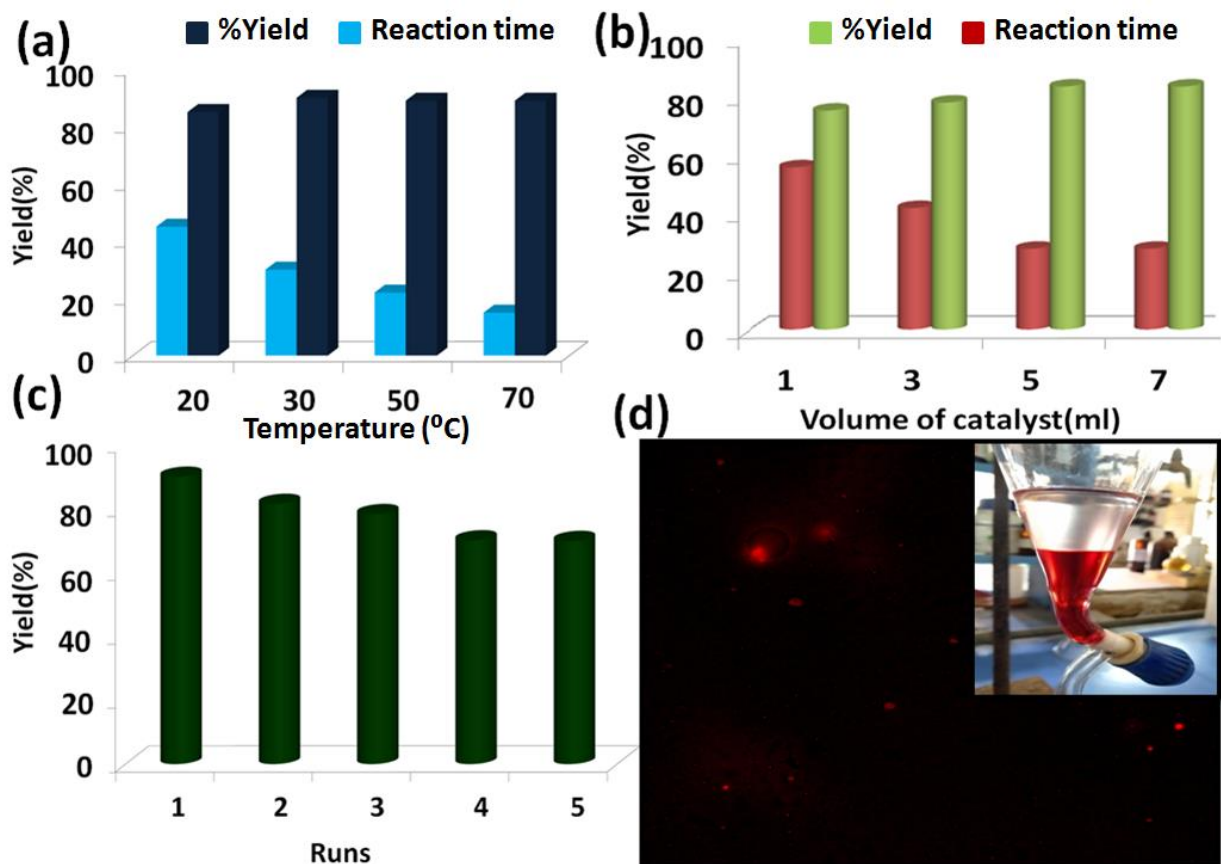
Figure 4.10 : Effect on time and yield for 2-(4-nitrophenyl)-benzimidazole formation using CuNPs@vesicles with variation in(a) reaction temperature(b) catalyst volume (c) recycling efficiency of the catalyst (d) florescent images of catalyst post recycling (Inset: Image showing regenerated catalyst)Reaction conditions for (a) o-phenylenediamine (1 mmol), 4-nitrobenzaldehyde (1 mmol), CuNPs@vesicles (1440 ppm, 5 ml) &15ml H_2O (b) o-phenylenediamine (1 mmol), 4-nitrobenzaldehyde (1 mmol), CuNPs@vesicles (1440 ppm), 30°C (c) o-phenylenediamine (1 mmol), 4-nitrobenzaldehyde (1 mmol), CuNPs@vesicles (1440 ppm, 5 ml), 30 °C.*Isolated yield.

The results could be understood in terms of increase in number of catalytically active Cu sites. The constant results beyond 5 ml of catalyst volume suggest the complete encapsulation of reactants in the CuNPs@vesicles. The reaction was also performed at different temperatures to understand the effect of temperature on the reaction performance.

It was found that increasing the reaction temperature had negligible effect on product yield (**Figure 4.10 (a)**). However, reaction times were reduced on increasing both the parameters. The reaction did not proceed in the absence of catalyst even after 3 h which highlights the potential role of the catalyst for the benzimidazole synthesis.

Thus, optimized reaction conditions derived from the above-mentioned studies were 5 ml CuNPs@vesicles at 30 °C in water. Under the optimized conditions 1:1 stoichiometric ratio of the reactants gave desired 2-substituted benzimidazoles which suggested that the catalyst is regioselective.

The scope of the reaction was extended to other substrates to synthesize a series of 2-substituted benzimidazole derivatives using o-PDA and various substituted aromatic benzaldehydes (**Table 4.5**). Interestingly, we observed that the substitution on aromatic aldehydes had an impact on the reaction time. Those aldehydes having EWG as substituents requires lower reaction times as compared to aldehydes with ERG. This is attributed to the reaction mechanism, wherein a nucleophilic attack of o-PDA on aromatic aldehyde consisting of EWG increases the electrophilicity of carbonyl carbon thus favoring the nucleophilic attack. It was, further, observed that the position of substituent also had an effect on reaction time, for instance the time taken for completion of reaction is 40 mins when the reactant is m-nitrobenzaldehyde (**Table 4.5, entry 2**) whereas it is 30 mins in case of p-nitrobenzaldehyde (**Table 4.5, entry 1**).
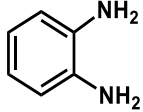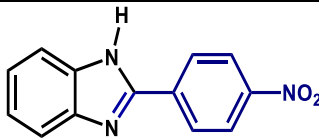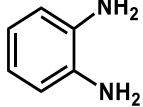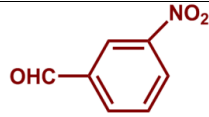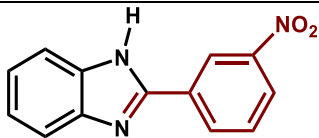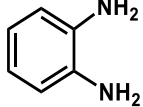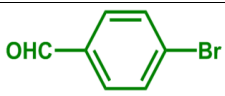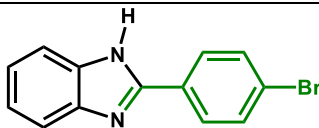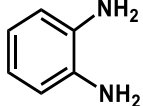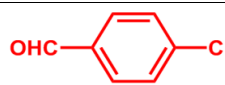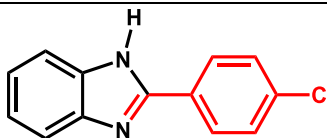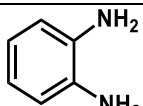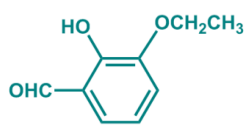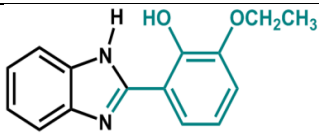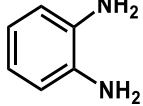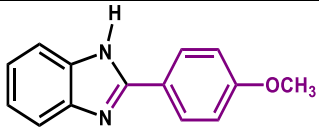
A time difference of 10 mins is related to the steric effect which also has an influence on the yield (86% for m-nitrobenzaldehyde and 90% for p-nitrobenzaldehyde). The reaction times in the present study are much lower which can be explained on the basis of the fact that CuNPs@vesicles are nanoreactors bearing catalytically active Cu (0) sites. The hydrophobic pockets inside the bilayer structure of CuNPs@vesicles encapsulate the substrates and enhance their concentration as well as proximity with catalytically active Cu (0) sites resulting in faster catalysis.

The environmental impact of this catalytic protocol was assessed through E-factor calculations which measures the amount of waste generated during a synthetic process. The environmental viability of this catalytic protocol was assessed in terms of E-factor calculated as per the following formula:

$$\text{E-factor} = \frac{\text{mass of waste generated during the reaction (in g)}}{\text{mass of the desired product formed (in g)}}$$

Since the catalyst was recovered for the usage in new reaction cycle the mass of catalyst has not been considered for the E-factor calculations. The values of E-factor have been calculated for the synthesis of all the benzimidazole derivatives and are given in **Table 4.5**. The E-factor values evaluated for the reactions were found to be in the range of 0.11-0.19 advocating green nature of the proposed protocol.

Table 4.5: Substrate scope of reaction as per scheme 3 by using o-PDA and substituted aromatic aldehydes via reduction of 2-Nitroaniline

| Sr. No.	Diamine	Aromatic aldehyde	Product	Time (mins)	Yield (%)	E-factor
1				30	90	0.11
2				40	86	0.16
3				60	88	0.14
4				45	85	0.18
5				70	84	0.18
6				60	84	0.19

Reaction conditions: o-phenylenediamine (1.0 mmol), aromatic aldehyde (1.0 mmol), CuNPs@vesicles (5 ml, 1440 ppm), water (15 ml), room temperature (30 ^{0}C). Isolated yield.

Table 4.6: Comparison of CuNPs@vesicles nanoreactors with some catalytic systems reported for benzimidazole synthesis

Sr. No	Catalyst	Time	Yield	Solvent	Temperature	Ref
1	CuI NPs	1h	96%	CH_3CN/O_2	RT	[45]
2	Pd/C	4h	66%	Chlorobenzene	80°C	[21]
3	$Mo_{72}V_{30}$nanocluster	3h	90%	$EtOH/O_2$	60°C	[22]
4	$CuFe_2O_4$ NPs	24 h	89%	$Toluene/O_2$	110°C	[27]
5	Bimetallic Cu-Mn B spinel oxide	12 h	20%	DMSO	110°C	[26]
6	CuNPs@vesicles	0.5h	90%	H_2O	30°C	**This Work**

4.4 Recycling and regeneration studies

Another advantage of present catalytic system over previous reports is its recyclability upto 5 cycles with a marginal decrease in the yield. The red metallovesicle solution, after the reduction reaction turns black, gets regenerated on treatment with ethyl acetate and dilution with water. The recycle red solution was used for benzimidazole synthesis.
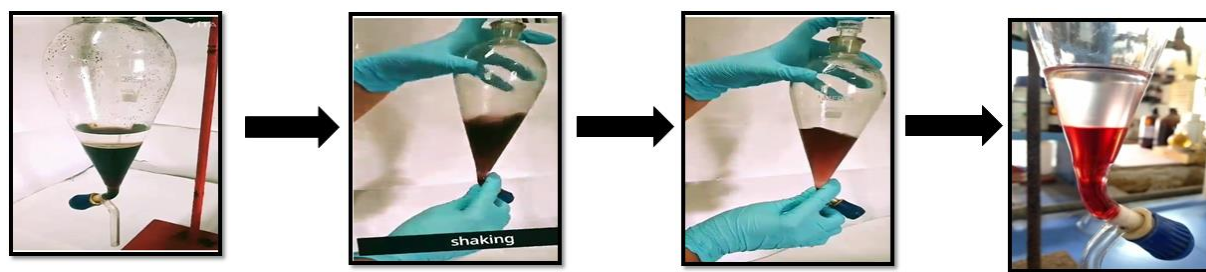

Figure 4.11: Regeneration of catalyst after reduction reaction

The florescent micrograph of recycled catalyst after 1st cycle showed spherical morphology indicative of the fact that the vesicles remain intact even after recycling as shown in **Figure 4.12.** Corroborative evidences from other analytical techniques like FTIR, UV-vis spectrophotometry, FEG-SEM analysis support the findings. FTIR confirms that the presence of peak corresponding to intrachain hydrogen bonding at 1641cm^{-1} and appearance of SPR band of CuNPs in the recycled catalyst confirming that catalyst remains intact. There is a substantial decrease in the reaction yield after 5th cycle owing to the distortion in vesicular structure which is evident from florescent

micrograph (**Figure 4.12(f)**). AAS analysis confirmed the absence of leached copper ions in the reaction mixture.
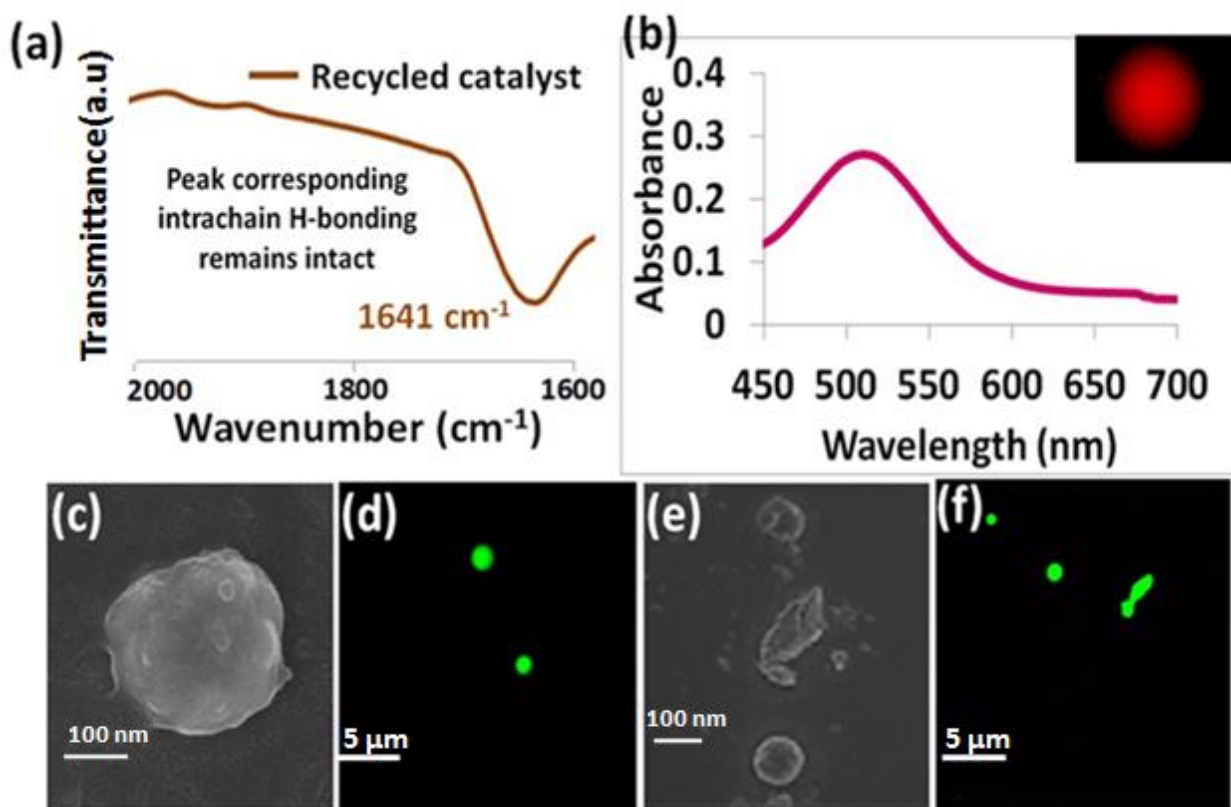

Figure 4.12:(a) FTIR spectrum (b) UV-vis spectrum of recycled catalyst (c) FEG-SEM image (d)florescent micrograph of catalyst after 1st recycling cycle (e) FEG-SEM image and (f) florescent micrograph of catalyst after 5th recycling cycle.

4.5 Plausible mechanism

A plausible mechanism was proposed to explain the phenomenon of catalysis. CuNPs@vesicles acts as nanoreactors for the transformation. These nanoreactors can entrap the reactants by the virtue of hydrophobic interactions and thus the reactions can be carried out in water instead of organic solvents. The fluorescence microscopy image of hydrophobic dye encapsulated vesicles provides evidence for their ability to entrap hydrophobic moieties (**Figure 4.6**). The nanoreactors are embellished with catalytically active CuNPs and when there is a confinement of reactant molecules in the vesicular bilayer these NPs come in close proximity with the reactants. Further the entrapment of reactant molecules inside the vesicular bilayer causes their concentration at the

active site thus causing a rapid catalysis (as shown in **Figure 4.13**).

This is evident from the experimental data which shows that low reaction time is required for complete formation of product. The Cu (0) sites in catalyst activate the carbonyl carbon of the aromatic aldehyde for nucleophilic attack by –NH$_2$ group of o-phenylenediamine. The imine formed was further attacked by second –NH$_2$ group resulting in the formation of dihydroimidazole followed by aromatization to give 2-aryl-1*H*-benzimidazoles as product.
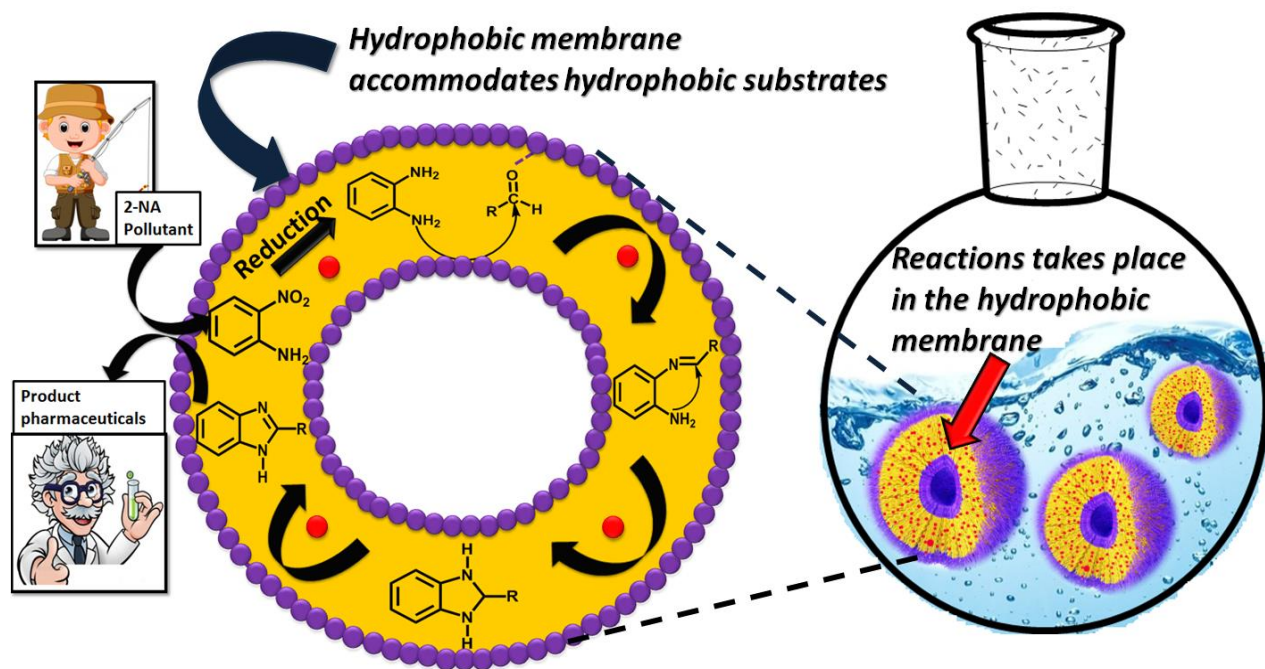
Figure 4.13: Probable mechanism of catalysis within the nanoreactors: the hydrophobic interior accommodates water insoluble organic substrates.

Recently Li *et. al.*, have reported a base free catalysis but by using palladium catalyst in toluene [46]. Herein, we report a convenient way to synthesize benzimidazole from *o*-nitroaniline and p-nitrobenzylalcohol catalyzed by CuNPs@vesicles.
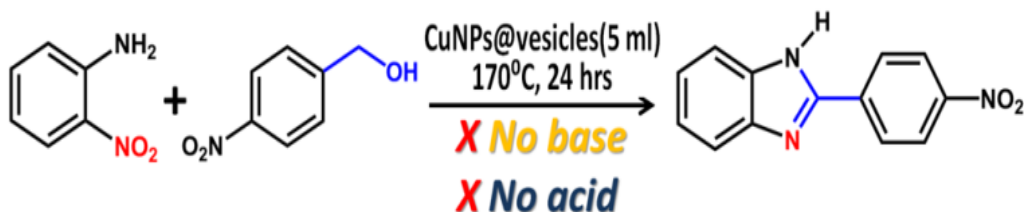
Scheme 4.4: Synthesis of 2-(4-Nitrophenyl)-1H-benzo[d]imidazole via dehydrogenative coupling of 2-nitoaniline and p-nitrobenzyl alcohol using CuNPs@vesicles

However, we successfully report the formation of desired product with 70% isolated yield using

in-expensive and recyclable copper catalyst in water, making the protocol relatively sustainable. The reaction did not proceed at lower temperatures, while at 150 °C traces of the product were obtained (**Table 4.7, entry 4**).

Table 4.7: Optimization of reaction condition (dehydrogenative coupling)

Sr. No.	Temperature (°C)	%Yield
1.	30	No conversion
2.	80	No conversion
3.	120	No conversion
4.	150	Trace
5.	170	70%

Reaction conditions: 2-nitroaniline (0.3 mmol), p-nitrobenzyl alcohol (0.9 mmol) and 5 mL catalyst.

Further increase in temperature to 170 °C gave 70% of desired product under base-free conditions. However extensive studies and optimizations are required to synthesize the product at lower temperatures using this catalyst which is a future prospect of the work.

4.6 Conclusions

To conclude, metallovesicles derived from an amphiphilic polymer and loaded with inexpensive metal nanoparticles were efficiently used as catalyst for cascade synthesis of 2-aryl-1H-benzimidazoles. The catalyst aided regioselective benzimidazole formation upon using two different approaches. It is remarkable that low level (1440 ppm) loadings resulted in good to excellent product yields. As successfully validated, upon employing CuNPs@vesicles as catalytic systems, the need for stoichiometric amounts of reagents and hazardous solvents can be eliminated.

Thus, the approach is environmentally benign, as the entire cascade of reactions proceeds in aqueous medium at ambient conditions. The important feature of regeneration and recyclability (upto 5 cascade cycles) can be attributed to the robust nature and stability of vesicular nanostructures. With appropriate optimizations it will be possible to extend the scope of

dehydrogenative coupling at ambient temperatures using substituted benzyl alcohols and o-nitroaniline.

4.7 References

[1]   S.A. Meeuwissen, A. Rioz-Martínez, G. De Gonzalo, M.W. Fraaije, V. Gotor, J.C.M. Van Hest, Cofactor regeneration in polymersome nanoreactors: Enzymatically catalysed Baeyer-Villiger reactions, J. Mater. Chem. 21 (2011) 18923–18926. https://doi.org/10.1039/c1jm12407b.

[2]   S. Khan, J. McCabe, K. Hill, P.A. Beales, Biodegradable hybrid block copolymer – lipid vesicles as potential drug delivery systems, J. Colloid Interface Sci. 562 (2020) 418–428. https://doi.org/10.1016/j.jcis.2019.11.101.

[3]   S.R. Mane, A. Sathyan, R. Shunmugam, Biomedical applications of pH-responsive amphiphilic polymer nanoassemblies, ACS Appl. Nano Mater. 3 (2020) 2104–21117. https://doi.org/10.1021/acsanm.0c00410.

[4]   D. Shi, X. Zhang, J. Wang, J. Fan, Highly reactive and stable nanoscale zero-valent iron prepared within vesicles and its high-performance removal of water pollutants, Elsevier B.V., 2018. https://doi.org/10.1016/j.apcatb.2017.09.057.

[5]   V. Kumar, D.G. Khandare, A. Chatterjee, M. Banerjee, DBSA mediated chemoselective synthesis of 2-substituted benzimidazoles in aqueous media, Tetrahedron Lett. 54 (2013) 5505–5509. https://doi.org/10.1016/j.tetlet.2013.07.147.

[6]   J.E. Moore, T.M. McCoy, A. V. Sokolova, L. de Campo, G.R. Pearson, B.L. Wilkinson, R.F. Tabor, Worm-like micelles and vesicles formed by alkyl-oligo(ethylene glycol)-glycoside carbohydrate surfactants: The effect of precisely tuned amphiphilicity on aggregate packing, J. Colloid Interface Sci. 547 (2019) 275–290. https://doi.org/10.1016/j.jcis.2019.03.068.

[7]   H. Sun, Q. Yang, J. Hao, Self-patterning porous films of giant vesicles of {Mo72Fe30}(DODMA)3 complexes as frameworks, Adv. Colloid Interface Sci. 235 (2016) 14–22. https://doi.org/10.1016/j.cis.2016.05.005.

[8]   R. Shankar, B. Jangir, A. Sharma, Palladium nanoparticles anchored on polymer vesicles as Pickering interfacial catalysts for hydrolytic oxidation of organosilanes, New J. Chem. 41 (2017) 8289–8296. https://doi.org/10.1039/c7nj01314k.

[9]   X. Li, S. Li, H. Zou, A. Song, J. Hao, Y.I. Lee, H.G. Liu, Block copolymer vesicles via liquid/liquid interface-mediated self-assembly, Appl. Surf. Sci. 499 (2020) 143896. https://doi.org/10.1016/j.apsusc.2019.143896.

[10] M. Schwarze, T. Pogrzeba, I. Volovych, R. Schomäcker, Microemulsion systems for catalytic reactions and processes, Catal. Sci. Technol. 5 (2015) 24–33. https://doi.org/10.1039/c4cy01121j.

[11] K. Holmberg, Organic and bioorganic reactions in microemulsions, Adv. Colloid Interface Sci. 51 (1994) 137–174. https://doi.org/10.1016/0001-8686(94)80035-9.

[12] Y. Wei, L. Wang, J. Huang, J. Zhao, Y. Yan, Multifunctional Metallo-Organic Vesicles Displaying Aggregation-Induced Emission: Two-Photon Cell-Imaging, Drug Delivery, and Specific Detection of Zinc Ion, ACS Appl. Nano Mater. 1 (2018) 1819–1827. https://doi.org/10.1021/acsanm.8b00226.

[13] H. Sun, J. Jiang, Y. Xiao, J. Du, Efficient Removal of Polycyclic Aromatic Hydrocarbons, Dyes, and Heavy Metal Ions by a Homopolymer Vesicle, ACS Appl. Mater. Interfaces. 10 (2018) 713–722. https://doi.org/10.1021/acsami.7b15242.

[14] Y. Zhu, L. Fan, B. Yang, J. Du, Multifunctional homopolymer vesicles for facile immobilization of gold nanoparticles and effective water remediation, ACS Nano. 8 (2014) 5022–5031. https://doi.org/10.1021/nn5010974.

[15] Y. Fu, L. Qin, D. Huang, G. Zeng, C. Lai, B. Li, J. He, H. Yi, M. Zhang, M. Cheng, X. Wen, Chitosan functionalized activated coke for Au nanoparticles anchoring: Green synthesis and catalytic activities in hydrogenation of nitrophenols and azo dyes, Appl. Catal. B Environ. 255 (2019) 117740. https://doi.org/10.1016/j.apcatb.2019.05.042.

[16] M. Wang, D. Tian, P. Tian, L. Yuan, Synthesis of micron-SiO 2 @nano-Ag particles and their catalytic performance in 4-nitrophenol reduction, Appl. Surf. Sci. 283 (2013) 389–395. https://doi.org/10.1016/j.apsusc.2013.06.120.

[17] S. Haider, T. Kamal, S.B. Khan, M. Omer, A. Haider, F.U. Khan, A.M. Asiri, Natural polymers supported copper nanoparticles for pollutants degradation, Appl. Surf. Sci. 387 (2016) 1154–1161. https://doi.org/10.1016/j.apsusc.2016.06.133.

[18] B. Shi, Y. Xu, T. Wang, S. Gao, G. Meng, K. Huang, Ag nanoparticles encapsulated in carboxyl-functionalized hollow microporous organic nanospheres for highly efficient catalysis applications, Appl. Catal. A Gen. 588 (2019) 117276. https://doi.org/10.1016/j.apcata.2019.117276.

[19] M.E. Mahmoud, M.F. Amira, M.E. Abouelanwar, S.M. Seleim, Catalytic reduction of nitrophenols by a novel assembled nanocatalyst based on zerovalent copper-nanopolyaniline-nanozirconium silicate, J. Mol. Liq. 299 (2020) 112192.

https://doi.org/10.1016/j.molliq.2019.112192.

[20] K. Tateyama, K. Wada, H. Miura, S. Hosokawa, R. Abe, M. Inoue, Dehydrogenative synthesis of benzimidazoles under mild conditions with supported iridium catalysts, Catal. Sci. Technol. 6 (2016) 1677–1684. https://doi.org/10.1039/c5cy01601k.

[21] Q. Guan, Q. Sun, L. Wen, Z. Zha, Y. Yang, Z. Wang, The synthesis of benzimidazoles via a recycled palladium catalysed hydrogen transfer under mild conditions, Org. Biomol. Chem. 16 (2018) 2088–2096. https://doi.org/10.1039/c8ob00323h.

[22] A. Khoshyan, M. Pourtahmasb, F. Feizpour, M. Jafarpour, A. Rezaeifard, Aerobic {Mo72V30} nanocluster-catalysed heterogeneous one-pot tandem synthesis of benzimidazoles, Appl. Organomet. Chem. 33 (2019) 1–9. https://doi.org/10.1002/aoc.4638.

[23] V.D. Nguyen, C.K. Nguyen, K.N. Tran, T.N. Tu, T.T. Nguyen, H. V. Dang, T. Truong, N.T.S. Phan, Zeolite imidazolate frameworks in catalysis: Synthesis of benzimidazoles via cascade redox condensation using Co-ZIF-67 as an efficient heterogeneous catalyst, Appl. Catal. A Gen. 555 (2018) 20–26. https://doi.org/10.1016/j.apcata.2018.02.007.

[24] K. Bahrami, M.M. Khodaei, A. Nejati, Synthesis of 1,2-disubstituted benzimidazoles, 2-substituted benzimidazoles and 2-substituted benzothiazoles in SDS micelles, Green Chem. 12 (2010) 1237–1241. https://doi.org/10.1039/c000047g.

[25] D. C. Cimarelli, M. D. Nicola, S. Diomedi, R.Giovannini, E.M. Hamprecht, R Properzi, F. Sorana, Efficient one-pot two catalyst system in the construction of 2- substituted benzimidazoles: synthesis of benzimidazo[1,2- c]quinazolines, Org. Biomol. Chem. (2015).

[26] R. Sharma, F.A. Sofi, P. Rana, P. V. Bharatam, Bimetallic Cu-Mn B spinel oxide catalyzed oxidative synthesis of 1,2-disubstituted benzimidazoles from benzyl bromides, New J. Chem. 43 (2019) 4013–4016. https://doi.org/10.1039/c8nj05504a.

[27] D. Yang, X. Zhu, W. Wei, N. Sun, L. Yuan, M. Jiang, J. You, H. Wang, Magnetically recoverable and reusable CuFe2O4 nanoparticle-catalyzed synthesis of benzoxazoles, benzothiazoles and benzimidazoles using dioxygen as oxidant, RSC Adv. 4 (2014) 17832–17839. https://doi.org/10.1039/c4ra00559g.

[28] M. Hulla, S. Nussbaum, A.R. Bonnin, P.J. Dyson, The dilemma between acid and base catalysis in the synthesis of benzimidazole from: O -phenylenediamine and carbon dioxide, Chem. Commun. 55 (2019) 13089–13092. https://doi.org/10.1039/c9cc06156h.

[29] C. Chaudhari, S.M.A.H. Siddiki, K.I. Shimizu, Acceptorless dehydrogenative synthesis of benzothiazoles and benzimidazoles from alcohols or aldehydes by heterogeneous Pt catalysts

under neutral conditions, Tetrahedron Lett. 56 (2015) 4885–4888. https://doi.org/10.1016/j.tetlet.2015.06.073.

[30] F. Ke, P. Zhang, C. Lin, X. Lin, J. Xu, X. Zhou, Synthesis of benzimidazoles by CuI-catalyzed three-component reaction of 2-haloaniline, ammonia and aldehyde in water, Org. Biomol. Chem. 16 (2018) 8090–8094. https://doi.org/10.1039/c8ob02172d.

[31] S. Senthilkumar, M. Kumarraja, A facile and highly chemoselective synthesis of 1,2-disubstituted benzimidazoles using hierarchical nanoporous material, Tetrahedron Lett. 55 (2014) 1971–1974. https://doi.org/10.1016/j.tetlet.2014.01.140.

[32] N. Kaur, S. Kaur, G. Kaur, A. Bhalla, S. Srinivasan, G.R. Chaudhary, Metallovesicles as smart nanoreactors for green catalytic synthesis of benzimidazole derivatives in water, J. Mater. Chem. A. 7 (2019) 17306–17314. https://doi.org/10.1039/c9ta05441c.

[33] R.R. Thakore, B.S. Takale, G. Casotti, E.S. Gao, H.S. Jin, B.H. Lipshutz, Chemoselective Reductive Aminations in Aqueous Nanoreactors Using Parts per Million Level Pd/C Catalysis, Org. Lett. 22 (2020) 6324–6329. https://doi.org/10.1021/acs.orglett.0c02156.

[34] P.S. Rathore, R. Patidar, T. Shripathi, S. Thakore, Magnetically separable core-shell iron oxide@nickel nanoparticles as high-performance recyclable catalysts for chemoselective reduction of nitroaromatics, Catal. Sci. Technol. 5 (2015) 286–295. https://doi.org/10.1039/c4cy00673a.

[35] P. Nariya, M. Das, F. Shukla, S. Thakore, Synthesis of magnetic silver cyclodextrin nanocomposite as catalyst for reduction of nitro aromatics and organic dyes, J. Mol. Liq. 300 (2020) 112279. https://doi.org/10.1016/j.molliq.2019.112279.

[36] J. He, Y. Liu, T. Babu, Z. Wei, Z. Nie, Ja3032295 1..4, (2012) 1–4. papers://078f6c0c-8070-48cf-a26f-997df9318c5a/Paper/p2625.

[37] T. Mondal, K. Dan, J. Deb, S.S. Jana, S. Ghosh, Hydrogen-bonding-induced chain folding and vesicular assembly of an amphiphilic polyurethane, Langmuir. 29 (2013) 6746–6753. https://doi.org/10.1021/la401008y.

[38] J. Shen, Z. Wang, D. Sun, C. Xia, S. Yuan, P. Sun, X. Xin, PH-Responsive Nanovesicles with Enhanced Emission Co-Assembled by Ag(I) Nanoclusters and Polyethyleneimine as a Superior Sensor for Al3+, ACS Appl. Mater. Interfaces. 10 (2018) 3955–3963. https://doi.org/10.1021/acsami.7b16316.

[39] S.M. Lee, H. Chen, C.M. Dettmer, T. V. O'Halloran, S.T. Nguyen, Polymer-caged lipsomes: A pH-responsive delivery system with high stability, J. Am. Chem. Soc. 129 (2007) 15096–15097.

https://doi.org/10.1021/ja070748i.

[40] L.B. Sagle, Y. Zhang, V.A. Litosh, X. Chen, Y. Cho, P.S. Cremer, Investigating the hydrogen-bonding model of urea denaturation, J. Am. Chem. Soc. 131 (2009) 9304–9310. https://doi.org/10.1021/ja9016057.

[41] J. Yang, Y. Hu, R. Wang, D. Xie, Nanoparticle encapsulation in vesicles formed by amphiphilic diblock copolymers, Soft Matter. 13 (2017) 7840–7847. https://doi.org/10.1039/c7sm01354j.

[42] C.S. Chen, Y.T. Lai, T.W. Lai, J.H. Wu, C.H. Chen, J.F. Lee, H.M. Kao, Formation of Cu nanoparticles in SBA-15 functionalized with carboxylic acid groups and their application in the water-gas shift reaction, ACS Catal. 3 (2013) 667–677. https://doi.org/10.1021/cs400032e.

[43] J.R. Deka, M.H. Lee, D. Saikia, H.M. Kao, Y.C. Yang, Confinement of Cu nanoparticles in the nanocages of large pore SBA-16 functionalized with carboxylic acid: Enhanced activity and improved durability for 4-nitrophenol reduction, Dalt. Trans. 48 (2019) 8227–8237. https://doi.org/10.1039/c9dt00248k.

[44] P.S. Rathore, R. Patidar, S. Thakore, Nanoparticle-supported and magnetically recoverable organic-inorganic hybrid copper(ii) nanocatalyst: A selective and sustainable oxidation protocol with a high turnover number, RSC Adv. 4 (2014) 41111–41121. https://doi.org/10.1039/c4ra06599a.

[45] P.L. Reddy, R. Arundhathi, M. Tripathi, D.S. Rawat, CuI nanoparticles mediated expeditious synthesis of 2-substituted benzimidazoles using molecular oxygen as the oxidant, RSC Adv. 6 (2016) 53596–53601. https://doi.org/10.1039/c6ra11678g.

[46] X. Li, R. Hu, Y. Tong, Q. Pan, D. Miao, S. Han, An efficient route for the synthesis of benzimidazoles via a hydrogen-transfer strategy between o-nitroanilines and alcohols, Tetrahedron Lett. 57 (2016) 4645–4649. https://doi.org/10.1016/j.tetlet.2016.09.018.
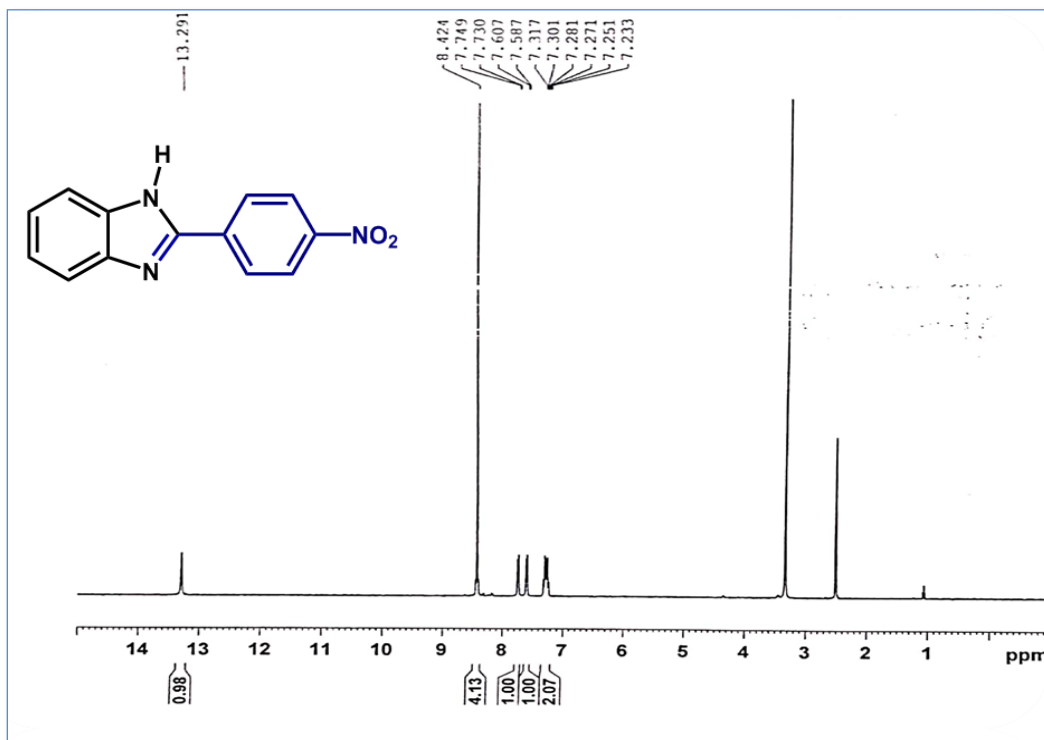
Spectral data

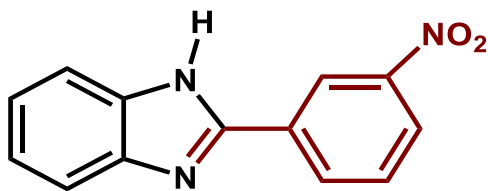**Entry S1: 2-(4-Nitrophenyl)-1H-benzo[d]imidazole**
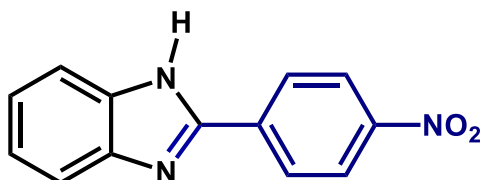
Color: Light red solid

Melting point: 318-320 °C

^{1}H NMR (DMSO-d6, 400 MHz) δ(ppm): 13.29 (s, 1H), 8.44-8.40 (m, 4H), 7.73 (d, J=7.6 Hz, 1H), 7.59 (d, J= 8.0 Hz, 1H), 7.23-7.31(m, 2H)
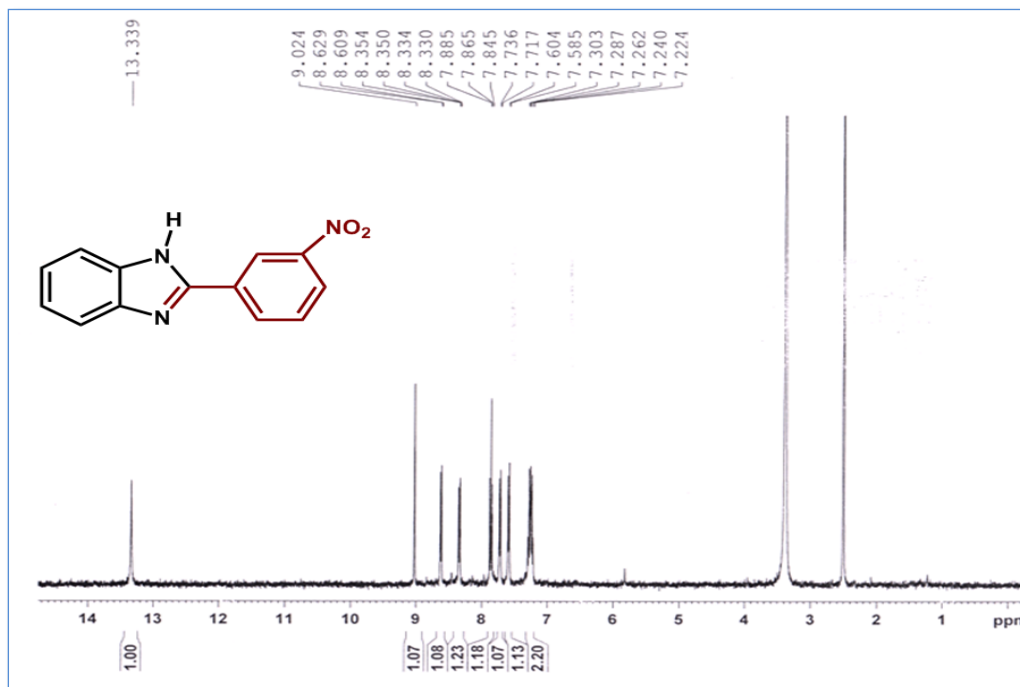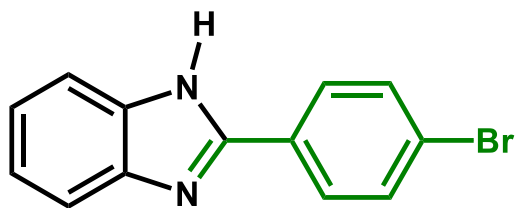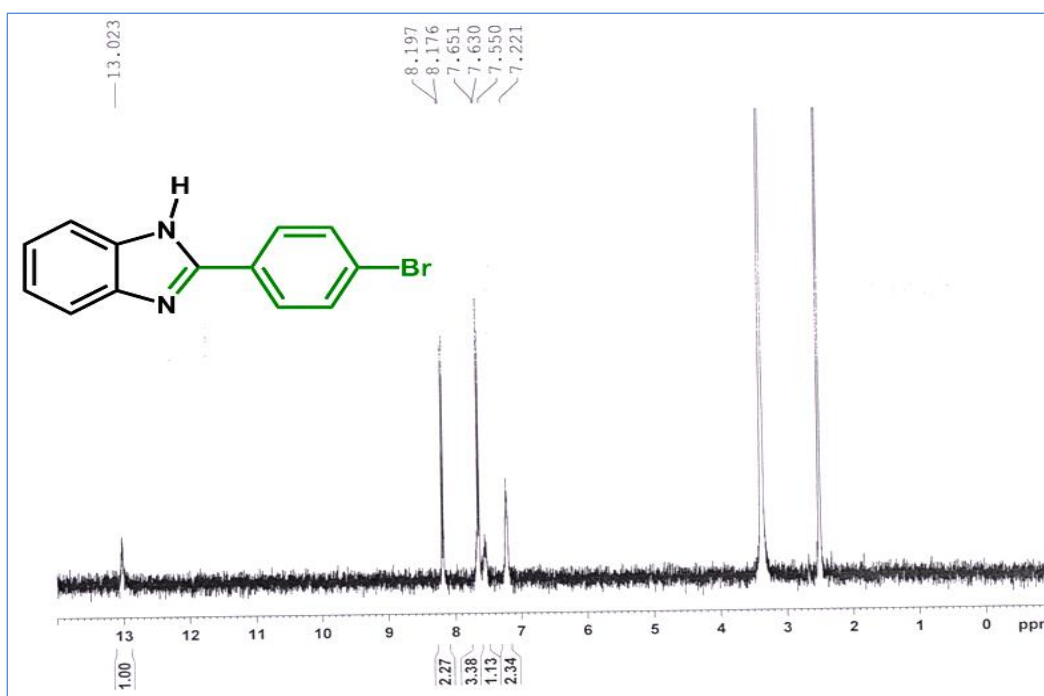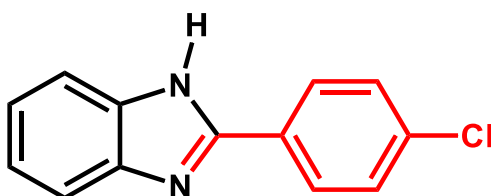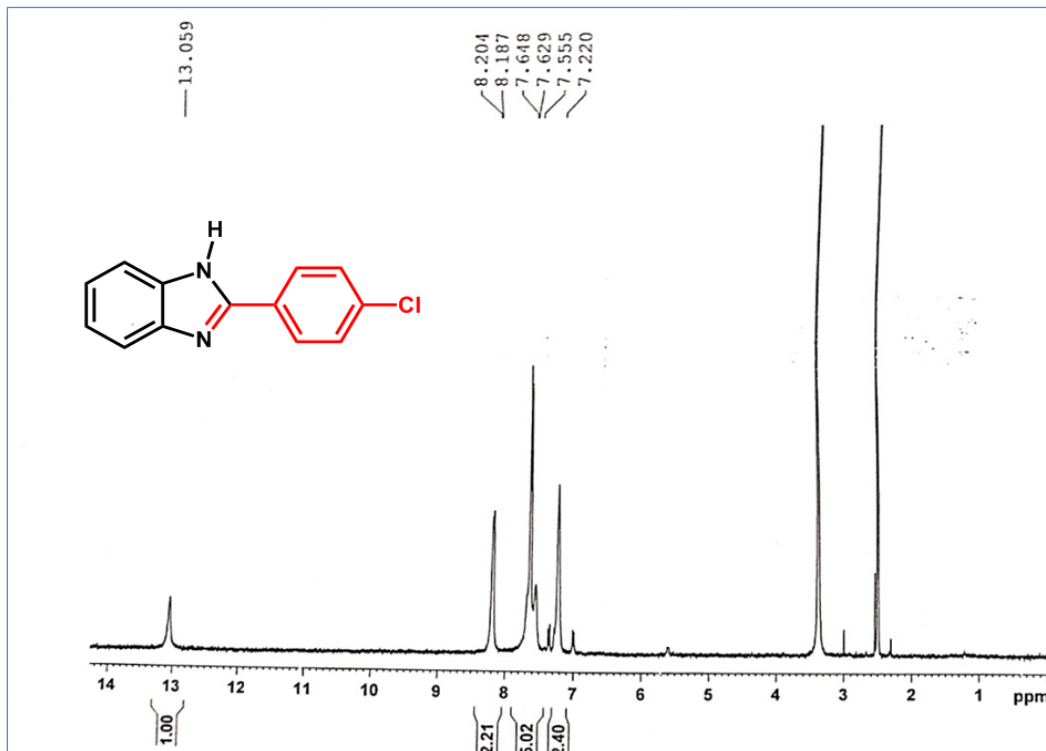

Figure S1:^{1}H NMR 2-(4-Nitrophenyl)-1H-benzo[d]imidazole

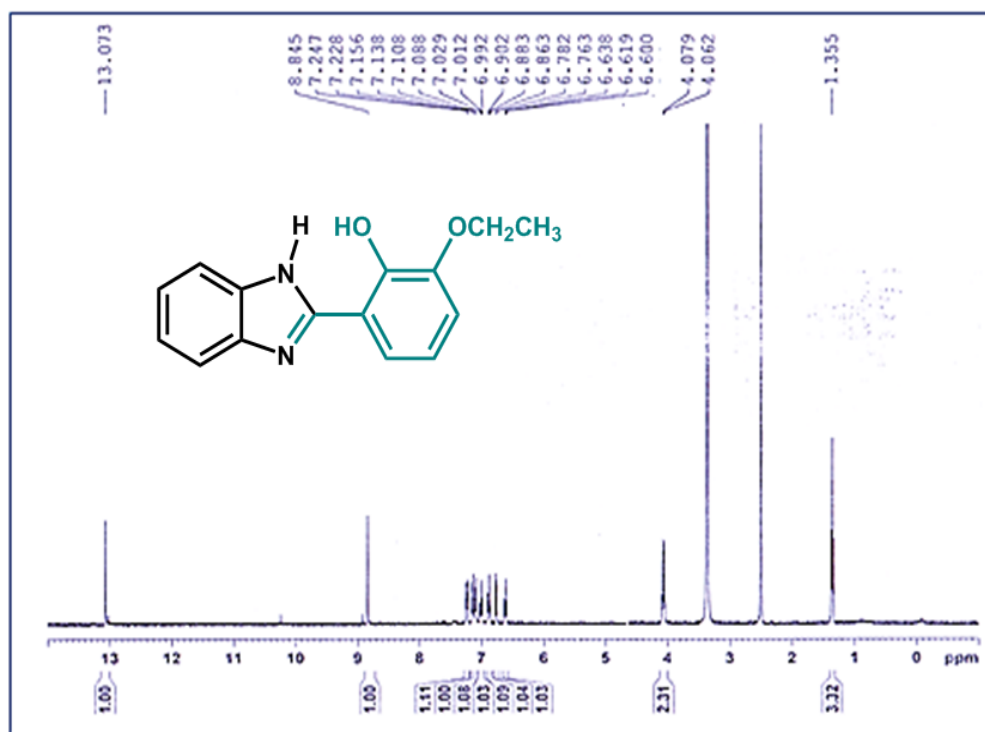**Entry S2: 2-(3-Nitrophenyl)-1H-benzo[d]imidazole**

Color: Yellow solid

Melting point: 201-203 °C

^{1}H NMR (DMSO-*d6*, 400 MHz) *δ*(ppm): 13.39 (s, 1H), 9.03 (s, 1H), 8.60-8.62 (d, J=8 Hz, 1H), 8.33-8.35 (m, 1H),7.84-7.88 (t, J=8 Hz, 1H),7.72 (d, J=7.6 Hz, 1H), 7.59 (d, J= 7.6 Hz,1H), 7.22-7.30 (m, 2H).

Figure S2: ^{1}H NMR of 2-(3-Nitrophenyl)-1H-benzo[d]imidazole

Entry S3: 2-(4-Bromophenyl)-1H-benzo[d]imidazole

Color: Off white solid

Melting point: 294-296 °C,

^{1}H NMR (DMSO-d6, 400MHz) δ(ppm):13.02(s, 1H), 8.17-8.19 (m, 2H), 7.55-7.65 (m, 4H), 7.22 (m, 2H).

Figure S3: ^{1}H NMR of 2-(4-Bromophenyl)-1H-benzo[d]imidazole

Entry S4: 2-(4-Chlorophenyl)-1H-benzo[d]imidazole

Colour: White solid

Melting point: 288-290 ℃,

¹H NMR (DMSO-d6, 400 MHz) δ(ppm): 13.05 (s, 1H), 8.19 (d, J=8.5 Hz, 2H), 7.64-7.55 (m, 4H), 7.22 (m, 2H).

Figure S4:¹H NMR of 2-(4-Chlorophenyl)-1H-benzo[d]imidazole

Entry S5: **2-(3-Ethoxy-2-hydroxyphenyl)-1H-benzo[d]imidazole**
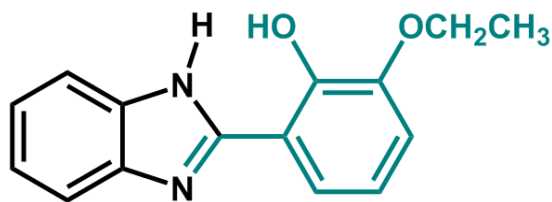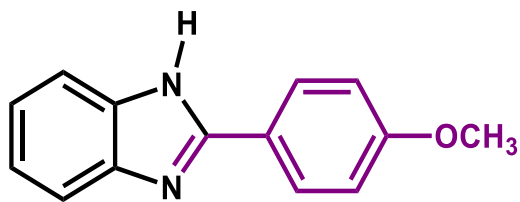
Colour: Yellow solid

Melting point: 350-370ºC

¹H NMR(DMSO-$d6$, 400 MHz) δ(ppm): 13.07 (s, 1H), 7.23 (d, J = 7.6 Hz, 1H), 7.14 (d, J = 7.2 Hz, 1H), 7.09(d, J = 8 Hz, 1H),7.01(t, J = 6.8 Hz,1H),6.88(t, J = 7.6 Hz, 1H),6.77(d, J = 7.6 Hz, 1H),6.61(t, J = 7.6 Hz, 1H), 4.07(q, J= 6.8 Hz,2H), 1.35(t, J =Hz , 3H).

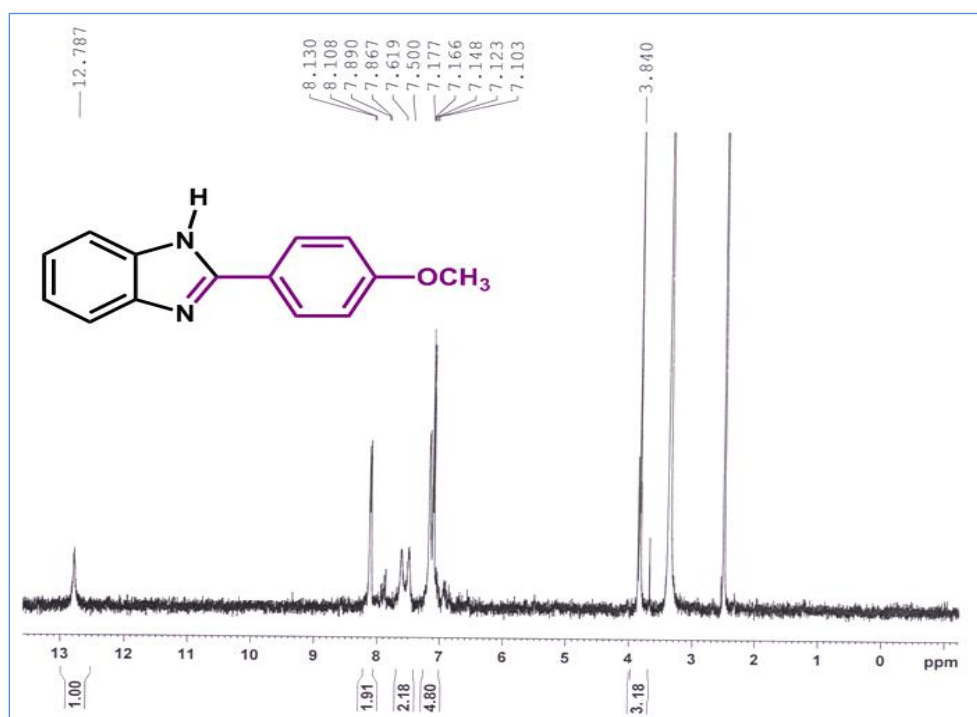**Figure S5:¹H NMR of 2-(3-Ethoxy-2-hydroxyphenyl)-1H-benzo[d]imidazole**

Entry S6: **2-(4-Methoxyphenyl)-1H-benzo[d]imidazole**
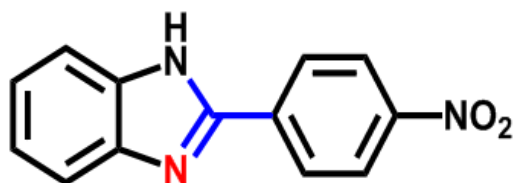
Color: Light yellow solid

Melting point: 221-223 °C

¹H NMR (DMSO-*d*6, 400 MHz) *δ*(ppm): 12.78 (s, 1H), 8.11 (d, *J* = 8.8 Hz, 2H), 7.50–7.89 (m, 2H), 7.10-7.17(m, 4H), 3.84 (s, 3H).

Figure S6:¹H NMR of 2-(4-Methoxyphenyl)-1H-benzo[d]imidazole

2-(4-Nitrophenyl)-1H-benzo[d]imidazole (TABLE 4.7, Entry 5)

Color: Light red solid

Melting point: 317-320 °C

1H NMR (DMSO-*d*6, 400 MHz) *δ*(ppm): 13.29 (s, 1H), 8.44-8.40 (m, 4H), 7.73 (d, J=7.6 Hz, 1H), 7.59 (d, J= 8.0 Hz, 1H), 7.23-7.31(m, 2H)
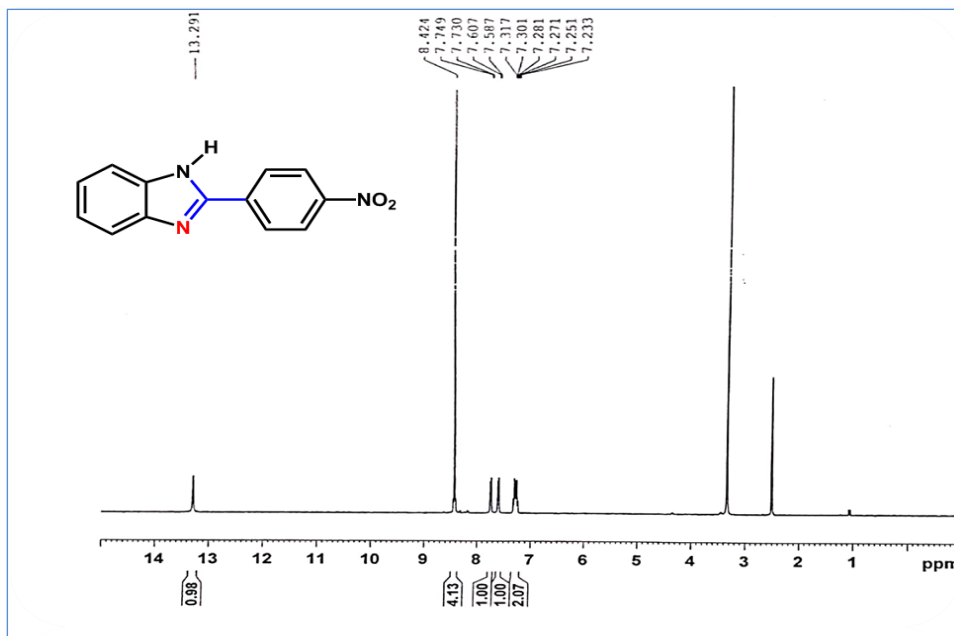

Figure S7:^{1}H NMR of 2-(4-Nitrophenyl)-1H-benzo[d]imidazole